SILICATE MELT PROPERTIES AND VOLCANIC ERUPTIONS

Youxue Zhang,[1,2] Zhengjiu Xu,[2] Mengfan Zhu,[1] and Haoyue Wang[1]

Received 15 October 2006; revised 6 March 2007; accepted 20 April 2007; published 5 December 2007.

[1] Knowledge about the properties of silicate melts is needed by volcanologists and petrologists to evaluate the dynamics of volcanic eruptions and magmatic processes. These properties include the solubility and diffusivity of volatile components in silicate melts, silicate melt viscosity, and the fragmentation condition. Data and models of each property are reviewed and assessed. For rhyolitic melts many properties are sufficiently well known to allow realistic modeling of volcanic and magmatic processes. One interesting example is the role of speciation in the solubility and diffusivity of H_2O and CO_2. Even though both H_2O and CO_2 are present in silicate melts as at least two species, the complexity in the solubility and diffusion behavior of H_2O and the simplicity of CO_2 are due to differences in the speciation reaction: For the H_2O component the stoichiometric coefficient is one for one hydrous species (molecular H_2O) but is two for the other hydrous species (OH) in the species interconversion reaction, whereas for CO_2 the stoichiometric coefficients for all carbon species are one. The investigation of the species reaction not only helps in understanding the solubility and diffusion behavior, but the reaction among the hydrous species also serves as a geospeedometer (cooling rate indicator) for hydrous rhyolitic pyroclasts and glass and provides a method to infer viscosity. For melts other than rhyolite, a preliminary description of their properties is also available, but much more experimental and modeling work is necessary to quantify these properties more accurately.

Citation: Zhang, Y., Z. Xu, M. Zhu, and H. Wang (2007), Silicate melt properties and volcanic eruptions, *Rev. Geophys.*, *45*, RG4004, doi:10.1029/2006RG000216.

1. INTRODUCTION

[2] Explosive volcanic eruptions are driven by exsolution of volatiles (mainly H_2O, with some CO_2 and other gases) that are initially dissolved in a melt (for clarity, melt means silicate liquid and glass hereinafter; magma includes melt plus phenocrysts, xenoliths, and/or gas bubbles). The development of an explosive volcanic eruption may be divided into two stages (Figure 1):

[3] 1. Oversaturation of dissolved volatiles in a melt leads to bubble nucleation and growth, which causes volume expansion, leading to eruption of bubbly magma. Oversaturation may be achieved by either magma ascent or removal of overlying rocks, both leading to decompression, or fractional crystallization, leading to an increase of volatile concentrations in the remaining melt. Modeling volcanic eruption dynamics in this stage requires quantification of bubble growth, which depends on volatile solubility and diffusivity as well as melt viscosity [*Proussevitch and Sahagian*, 1998].

[4] 2. The bubbly magma fragments to become an explosive gas flow carrying magma particles. Fragmentation is a critical moment in an eruption. Before fragmentation a volcanic eruption is a magma flow; after fragmentation the eruption becomes a gas flow with a major change of dynamics. Prediction of magma fragmentation requires knowledge of the fragmentation condition. In fragmentation criteria (see section 6) it is necessary to know pressure inside a bubble, meaning bubble growth must be modeled well. The dynamics of postfragmentation gas flow carrying magma particles depends critically on the mass fraction of the gas phase, which also depends on bubble growth rate in the first stage, as well as volatile loss from magma particles carried by the gas.

[5] In summary, solubility and diffusivity of volatile components (H_2O and CO_2) in natural silicate melts, melt viscosity, and fragmentation are important properties in understanding volcanic eruptions and other magmatic processes. These melt properties are reviewed and assessed in this paper. In addition, the hydrous species geospeedometer that is applicable to the investigation of the cooling rate of pyroclasts and in volcanic eruption columns will also be

[1]Ministry of Education Laboratory of Orogenic Belts and Crustal Evolution, School of Earth and Space Sciences, Peking University, Beijing, China.

[2]Department of Geological Sciences, University of Michigan, Ann Arbor, Michigan, USA.

8755-1209/07/2006RG000216
Paper number 2006RG000216

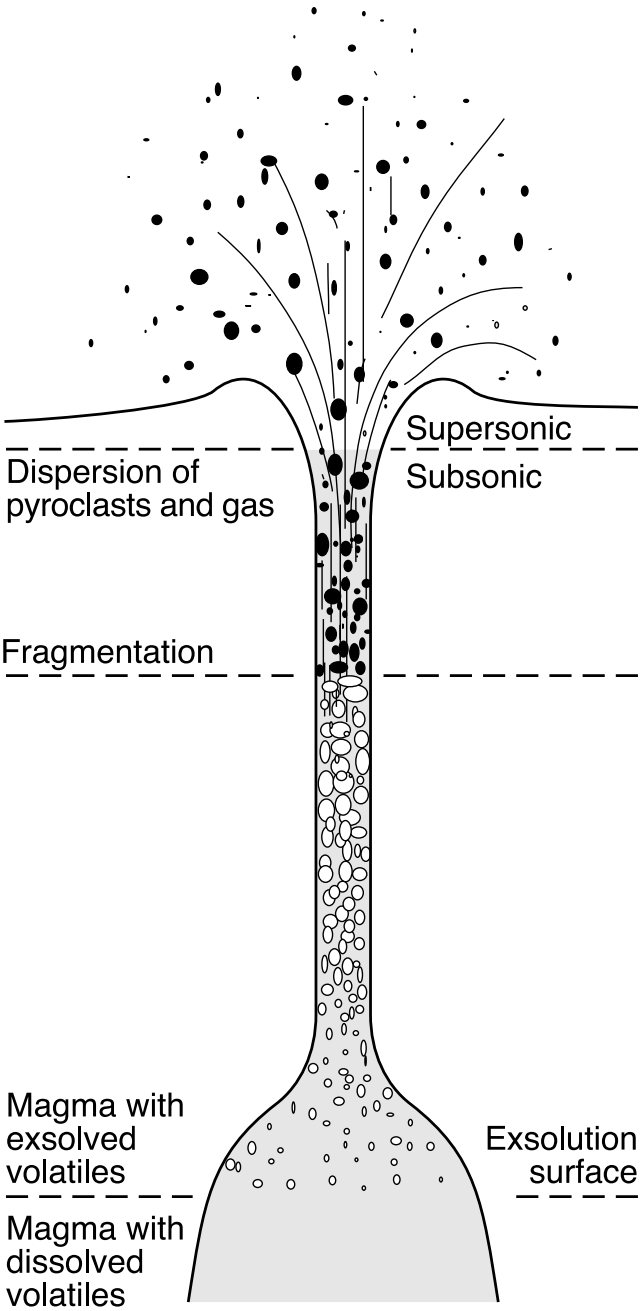

Figure 1. Dynamic stages of an explosive eruption. Initially, there are dissolved volatile components (mostly H_2O) in magma. When supersaturation of the volatiles is reached at the exsolution "surface," bubbles form and grow. As the magma ascends, bubble growth and new bubble formation increase the volume fraction of bubbles (vesicularity). At some critical point, fragmentation occurs, in which bubbles break up and release the gas. Hence a bubbly magma flow (magma is the continuous phase) changes into a gas flow carrying magma particles (gas is the continuous phase). Fragmentation is the transition from a nonexplosive liquid eruption to an explosive gas eruption. After *Wilson* [1980] and from *Zhang* [2004].

reviewed. Among different melts, properties of rhyolitic melt are the best understood, which allows realistic modeling of the dynamics of volcanic eruptions and magma chamber processes. For other melts, there are also some data, but more experimental and modeling efforts are necessary.

2. H_2O AND CO_2 SOLUBILITY

2.1. H_2O Speciation in Silicate Melts

[6] Before a discussion of H_2O solubility and diffusivity it helps to briefly outline H_2O speciation in silicate melts. For CO_2, understanding its speciation is less critical to its solubility but helps in understanding its diffusion. Hence CO_2 speciation will be discussed in section 3.2.

[7] The H_2O component dissolves in silicate melts as at least two species [*Stolper*, 1982a, 1982b], molecular H_2O (hereinafter referred to as H_2O_m, total H_2O content will be referred to as H_2O_t) and hydroxyls (hereinafter referred to as OH). The two species can be easily seen in infrared and Raman spectra [*Stolper*, 1982a; *Ihinger et al.*, 1994]. Infrared spectroscopy has been calibrated for quantitative measurement of species concentrations [e.g., *Newman et al.*, 1986; *Dixon et al.*, 1988; *Zhang et al.*, 1997a; *Ohlhorst et al.*, 2001; *Mandeville et al.*, 2002; *Leschik et al.*, 2004], but the accuracy of the calibration (about 5–10% relative) still does not match the high reproducibility of IR band intensity measurement (about 1% relative).

[8] The two hydrous species (H_2O_m and OH) interconvert in a silicate melt through the following homogeneous reaction (meaning that the reaction occurs within a single phase):

$$H_2O_m(\text{melt}) + O(\text{melt}) \rightleftharpoons 2OH(\text{melt}), \tag{1}$$

where O means anhydrous oxygen. By convention, the charges (such as O^{2-} and OH^-) are neglected because O often denotes bridging oxygen, but O^{2-} often denotes free oxygen anion. The equilibrium constant is denoted as K_2 (to distinguish it from other equilibrium constants, such as K_{22} in section 3.2):

$$K_2 = \frac{[OH]^2}{[H_2O_m][O]}, \tag{2}$$

where brackets mean activities approximated by mole fractions on a single oxygen basis [*Stolper*, 1982b; *Zhang*, 1999a]. The stoichiometric coefficient of 2 in front of OH in reaction (1) means that OH concentration is squared in equation (2). Hence OH concentration is not proportional to H_2O_m concentration; rather, the square of OH concentration is proportional to H_2O_m concentration (equation (2)). Calculations of species concentrations as a function of H_2O_t (Figure 2) show that (1) OH is the dominant species at low H_2O_t, but H_2O_m becomes the dominant species at high H_2O_t ($\geq$5 wt %, depending on the value of K_2) and (2) the ratio of H_2O_m/H_2O_t is roughly proportional to H_2O_t at small H_2O_t (<2 wt %) and then flattens (the ratio cannot exceed 1).

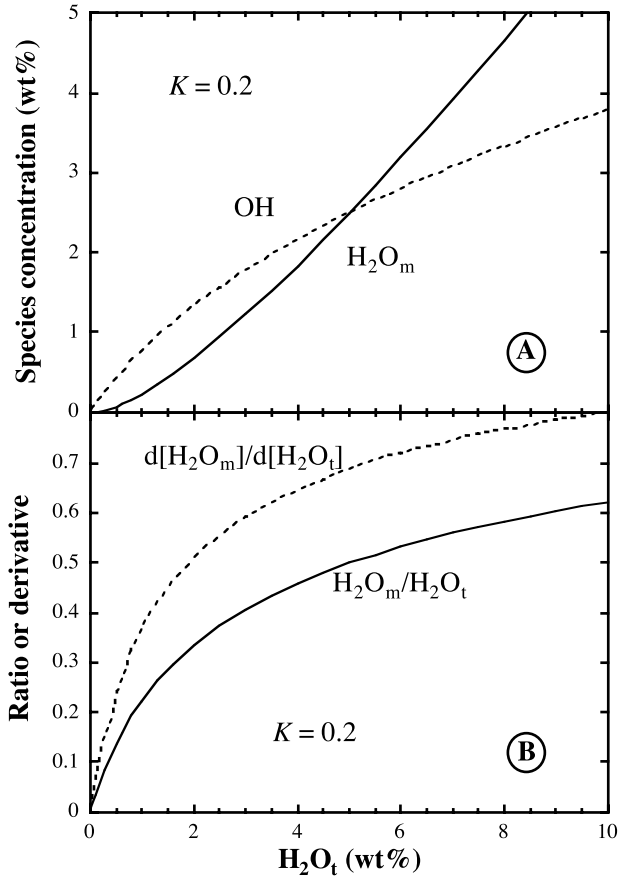

Figure 2. (a) Calculated H_2O species concentrations and (b) H_2O_m/H_2O_t ratio and the derivative $d[H_2O_m]/d[H_2O_t]$ as a function of H_2O_t. K_2 = 0.2 roughly corresponds to equilibrium at 892 K.

[9] The consequence of the seemingly simple fact of nonunity stoichiometric coefficient for OH in reaction (1) is the basis for many complexities in H_2O solubility and diffusivity and hence is the key for understanding these behaviors. For example, the solubility of most gas components in a silicate melt at low pressures is roughly proportional to the pressure of the gas component but not for H_2O. In terms of diffusion, for most components the diffusivity is roughly independent of its own concentration when the concentration is low, whereas H_2O_t diffusivity is roughly proportional to H_2O_t concentration at low H_2O_t. For CO_2, although there are also two species, there is no such complexity because the concentrations of the two species are proportional to each other (see section 3.2).

2.2. H_2O and CO_2 Solubility in Rhyolitic Melt

[10] Numerous experiments have been carried out to investigate the solubility of H_2O [*Goranson*, 1931; *Burnham and Jahns*, 1962; *Friedman et al.*, 1963; *Kadik et al.*, 1972; *Khitarov and Kadik*, 1973; *Shaw*, 1974; *Silver et al.*, 1990; *Ihinger*, 1991; *Holtz et al.*, 1992, 1995; *Blank et al.*, 1993; *Moore et al.*, 1995, 1998; *Dingwell et al.*, 1997; *Gardner et al.*, 1999; *Schmidt et al.*, 1999; *Yamashita*, 1999; *Mangan and Sisson*, 2000; *Behrens and Jantos*, 2001; *Tamic et al.*, 2001; *Liu et al.*, 2005] and CO_2 [*Fogel and Rutherford*, 1990; *Blank et al.*, 1993; *Tamic et al.*, 2001] in rhyolitic and quasi-rhyolitic melts. On the basis of the data many solubility models have been constructed [e.g., *Burnham*, 1975; *Silver and Stolper*, 1985; *Ihinger*, 1991; *Blank et al.*, 1993; *Holloway and Blank*, 1994; *Moore et al.*, 1995, 1998; *Papale*, 1997, 1999a; *Zhang*, 1999a; *Newman and Lowenstern*, 2002; *Liu et al.*, 2005; *Papale et al.*, 2006].

[11] Because of reaction (1) the dependence of H_2O solubility on pressure is somewhat complicated. The solubility of total H_2O may be written as

$$[H_2O_t] = [OH]/2 + [H_2O_m], \tag{3}$$

where brackets denote mole fractions of the dissolved species in the melt. From the vapor-melt equilibrium of H_2O (vapor) $\rightleftharpoons$ H_2O_m (melt) and assuming ideal gas behavior for the vapor phase and ideal mixing in the melt, $[H_2O_m]$ is proportional to P_{H2O}. From equation (2), [OH] is proportional to square root of $[H_2O_m]$ and hence is proportional to $P_{H_2O}^{1/2}$. Therefore H_2O_t solubility in silicate melt depends on pressure as

$$[H_2O_t] = k_1 P_{H_2O}^{1/2} + k_2 P_{H_2O}, \tag{4}$$

where the first term on the right-hand side accounts for OH species and the second term accounts for H_2O_m. Hence the solubility of H_2O does not follow a simple Henry's law, whereas that of CO_2 follows Henry's law (see below). The complicated behavior of H_2O solubility is not due to nonideality but is due to speciation and the factor of 2 for OH in reaction (1). According to equation (4), at low pressures ($\leq$50 MPa) the dissolved H_2O_t is low, meaning that OH is dominant (Figure 2), leading to H_2O_t solubility proportional to the square root of P_{H_2O}. As pressure increases, the dissolved H_2O_t increases, meaning increasing importance of H_2O_m and hence more rapid increase of the solubility with pressure than the square root dependence with pressure.

[12] Even though modeling solubility data is often a simple curve-fitting problem, careful consideration is still necessary. Below is a seemingly trivial but often overlooked point. Many authors conduct H_2O solubility experiments in the pressure range of 10 to 200 MPa. Some data in this pressure range are shown in Figure 3a by plotting weight percent of dissolved H_2O_t as a function of square root of pressure. Because the data conform well to a linear trend, one might be tempted to fit the data by a straight line with two fitting parameters:

$$C_w = a + bx, \tag{5}$$

where C_w is weight percent of H_2O_t (e.g., for 2 wt % H_2O_t, C_w = 2), $x = P^{1/2}$, and a and b are two fitting parameters. A fit by equation (5) is shown as dashed line in Figure 3b. It is not uncommon to see such a fit in publications, but it does not satisfy the condition that the solubility is zero when P = 0. Hence fitting by equation (5) may be used for interpolation but not for extrapolation to either lower or

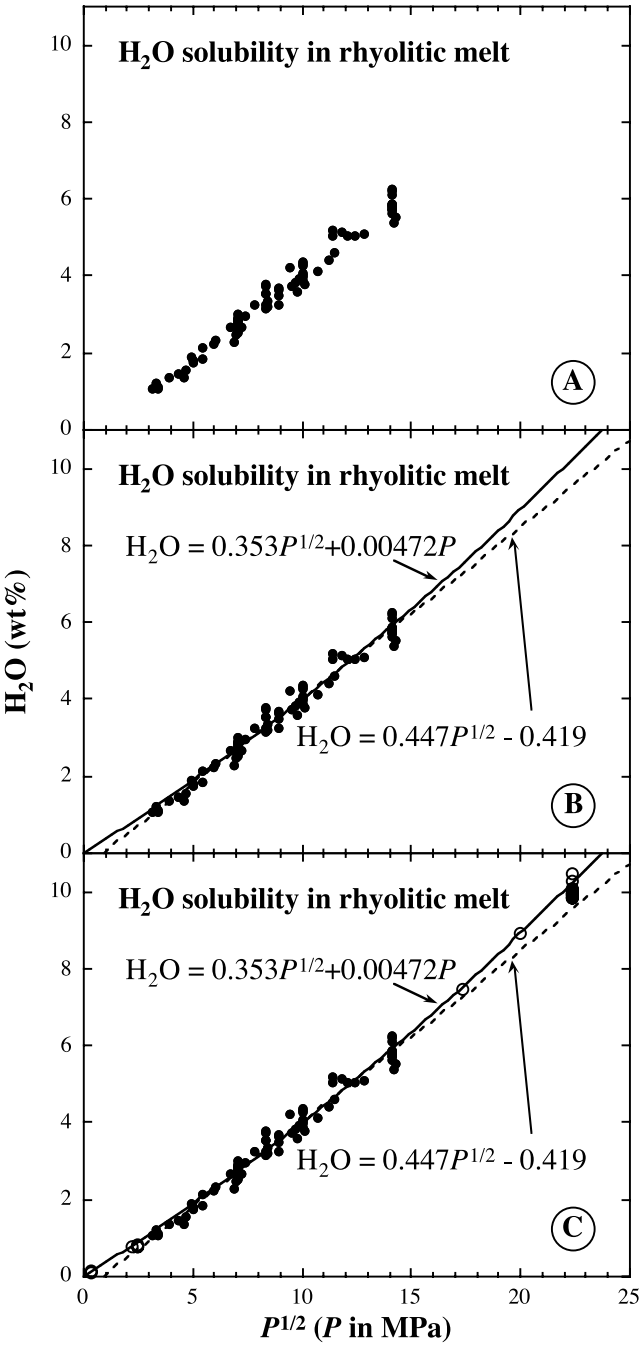

Figure 3. H_2O solubility data in rhyolitic melt at 1073–1123 K [*Silver et al.*, 1990; *Holtz et al.*, 1995; *Gardner et al.*, 1999; *Behrens and Jantos*, 2001; *Tamic et al.*, 2001] and fits. A small range of temperature (instead of a single temperature) is chosen so that there are enough data to cover both high and low pressures. Outlier points are excluded. (a) H_2O solubility data at pressures of 10–200 MPa (solid circles). (b) Two fits to the solubility data. (c) Fits compared with H_2O solubility data at both lower and higher pressures (open circles).

higher pressures. Another two-parameter equation to fit the solubility data is

$$C_w = ax + bx^2, \tag{6}$$

where x is again $P^{1/2}$ and a and b are two fitting parameters, which fits the data equally well and satisfies the limiting condition that the solubility is zero when $P = 0$ (solid curve in Figure 3b). When lower-pressure data (0.1–10 MPa) and higher-pressure (from 200 to 500 MPa) data are plotted as open circles in Figure 3c, it can be seen that the fit by equation (5) deviates from the experimental data at both higher and lower pressures, but the fit by equation (6) agrees well with the experimental data, meaning that it can be extrapolated to both higher and lower pressures. The ability of equation (6) to extrapolate to pressures lower than the experimental pressure range of 10–200 MPa is almost guaranteed because by adding the natural data point of (0, 0), prediction of low-pressure solubility is interpolation between (0, 0) and other data points. The ability of equation (6) to extrapolate to higher pressures (>200 MPa) is somewhat coincidental because the two terms on the right-hand side of equation (6) correspond to the theoretical solubility equation (equation (4)). Hence the relation has a theoretical basis, although it is not a rigorous thermodynamic model (e.g., fugacity is not used).

[13] In summary, when fitting experimental data after laborious work and examining how the property depends on some parameter, it helps to include the "free" data (the natural constraints). This is important not only for modeling solubility but also for viscosity [*Zhang et al.*, 2003], diffusivity, and other parameters.

[14] In addition to simple fits of the solubility data, more sophisticated models have been advanced, many requiring the calculation of fugacity [e.g., *Silver and Stolper*, 1985; *Blank et al.*, 1993; *Holloway and Blank*, 1994; *Moore et al.*, 1995, 1998; *Papale*, 1997, 1999a; *Zhang*, 1999a; *Newman and Lowenstern*, 2002]. Although the thermodynamic rigor is appreciated, such models are often considered too complicated to be included in eruption dynamics programs by the volcanological community, who would like one-line equations (or a few lines) to calculate solubility in software codes of eruption dynamics. For easy use by the volcanological community, *Liu et al.* [2005] constructed the following model to calculate the solubility of H_2O and CO_2 in rhyolitic and quasi-rhyolitic melts at 973–1473 K and 0–500 MPa:

$$C_w = \frac{354.94\sqrt{P_w} + 9.623P_w - 1.5223P_w^{3/2}}{T} + 0.0012439P_w^{3/2} + P_{CO_2}\left(-1.084\times10^{-4}\sqrt{P_w} - 1.362\times10^{-5}P_w\right) \tag{7}$$

$$C_{CO_2} = P_{CO_2}\left[\frac{(5668 - 55.99P_w)}{T} + \left(0.4133\sqrt{P_w} + 0.002041P_w^{3/2}\right)\right], \tag{8}$$

where C_w is total dissolved H_2O content in weight percent, C_{CO_2} is CO_2 concentration in weight ppm, T is temperature in kelvins, $P_w = X_w^g P$ and $P_{CO_2} = X_{CO_2}^g P$, P is total pressure in MPa, and X_w^g and $X_{CO_2}^g$ are mole fractions of H_2O and CO_2 gas in the gas phase. Comparison between data and

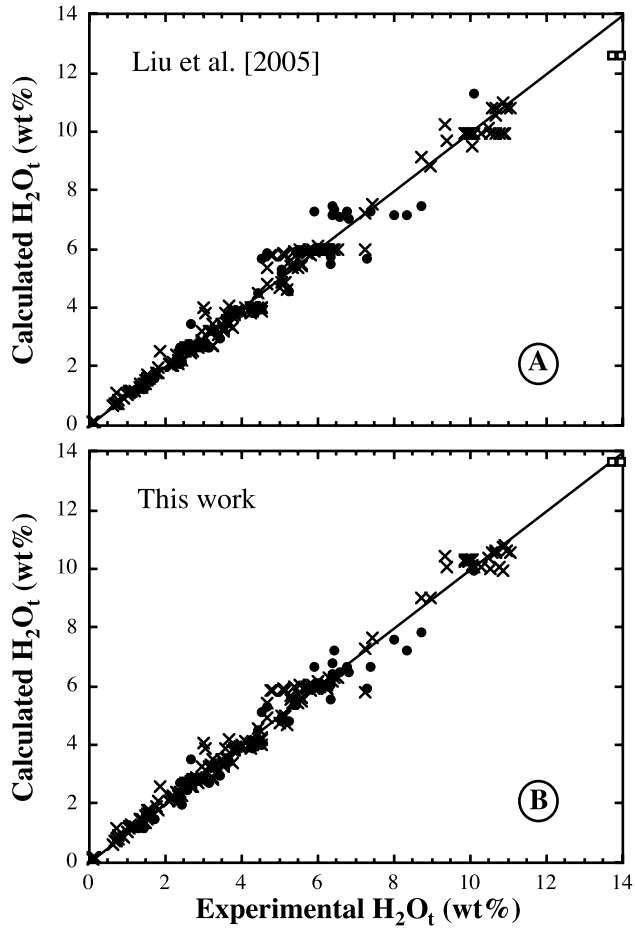

Figure 4. Comparison of two solubility models with experimental data: (a) *Liu et al.* [2005] and (b) this work. Experimental data are shown as crosses (data used in the model of *Liu et al.* [2005] for H_2O solubility in silicic melts below 500 MPa), open squares (solubility data in silicic melts at 800 MPa [*Holtz et al.*, 1995]), and solid circles (solubility data used in the model of *Moore et al.* [1998]).

model prediction is shown in Figure 4a. From equation (8) the solubility of CO_2 follows Henry's law (meaning the solubility is proportional to the partial pressure of CO_2), and the expression inside the bracket is Henry's law constant. *Liu et al.* [2005] compared this simple model with previous models (including the sophisticated models) and showed that the simple model reproduces experimental solubility data equally well or better than previous models in the range of 973–1473 K and 0–500 MPa. Hence the above formulations are recommended for the calculation of H_2O and CO_2 solubilities in rhyolitic melts in equilibrium with a CO_2-H_2O vapor phase (including pure end-members) in the applicable temperature and pressure range. However, there is a peculiar behavior in experimental CO_2 solubility data in rhyolite coexisting with an H_2O-CO_2 mixed vapor: CO_2 solubility apparently decreases as the CO_2 fraction in the vapor phase increases from 95 to 100% at 500 MPa. This behavior is well fit by equation (8) but may not be real. Additional data are needed to check the behavior in this range.

2.3. H_2O and CO_2 Solubility in Other Melts

[15] To the first order the solubility of H_2O and CO_2 does not depend strongly on silicate melt composition. For example, Figure 5 shows that H_2O solubility in basaltic melt (solid circles) is not much different from that in rhyolitic melt (open circles) at 1473 K, especially at low pressures. Previously, solubility comparison was often made between rhyolite at 1123 K (dashed curve) and basalt at 1473 K (solid circles), where the difference is larger (Figure 5). Figure 4a also compares the solubility data in basaltic and intermediate melts (solid circles, data given by *Moore et al.* [1998]) with calculated solubility in rhyolitic melt using the model of *Liu et al.* [2005], and the difference is small. Hence, for rough calculation of H_2O and CO_2 solubility of other melts the model of *Liu et al.* [2005] may also be used. An even simpler estimate of CO_2 solubility at magmatic temperatures and $P_{CO_2} \leq 500$ MPa is about 5 ± 1 ppm per MPa of P_{CO_2}.

[16] *Newman and Lowenstern* [2002] constructed a solubility model for H_2O-CO_2 in both basalt and rhyolite. The code is available from a Web server (http://www.iamg.org/CGEditor/index.htm). For melts of general compositions such as intermediate melt compositions, two recent models have been advanced [*Moore et al.*, 1998; *Papale et al.*, 2006]. The model of *Moore et al.* [1998] is for solubility of H_2O only and takes the following form:

$$2\ln X_{H_2O}^{melt} = \frac{a}{T} + (b_{Al_2O_3}X_{Al_2O_3} + b_{FeO_t}X_{FeO_t} + b_{Na_2O}X_{Na_2O})\frac{P}{T} + c\ln f_{H_2O}^{fluid} + d, \quad (9)$$

where a = (2565 ± 362) K, b_{Al2O3} = −(1.997 ± 0.706) K bar^{-1}, b_{FeOt} = −(0.9275 ± 0.394) K bar^{-1}, $b_{Na_2}O$ = (2.736 ±

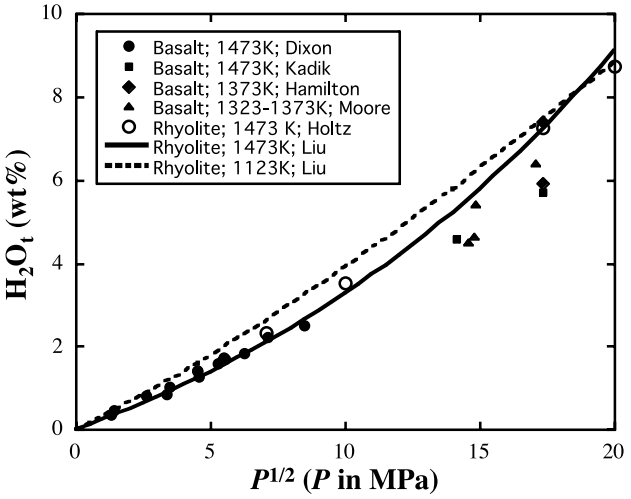

Figure 5. Comparison of H_2O solubility in basaltic melt (solid circles, squares, diamond, and triangles) and in rhyolitic melt (open circles and calculated curves). Experimental data are from *Dixon et al.* [1995], *Kadik et al.* [1972], *Hamilton et al.* [1964], *Moore et al.* [1998], and *Holtz et al.* [1995]. Calculated curves are based on the model of *Liu et al.* [2005].

0.871) K bar^{-1}, $c = 1.117 \pm 0.069$, $d = -14.21 \pm 0.54$, X_i is oxide mole fraction of the component, pressure and fugacity (f) are in bars, temperature is in kelvins, and fugacity of H_2O in the fluid is calculated using the model of *Holloway and Blank* [1994], which is based on the Redlich-Kwong equation of state. In equation (9), only three oxide components are included because the effects of the other components were found to be negligible. Comparison with experimental data shows that the model is applicable to pressures of 1–300 MPa but not at $\leq$1 MPa such as the atmospheric pressure of 0.1 MPa [*Liu et al.*, 2005]. The model of *Papale et al.* [2006], which supersedes that of *Papale* [1999a], is for the solubility of both H_2O and CO_2 and considers the compositional effects of all major melt components using a regular solution model. The model is general but is not intended to match the accuracy of models on a single melt composition. By comparison with experimental data the model of *Papale et al.* [2006] was found to apply well to intermediate pressures of 10–300 MPa but did not apply well outside the pressure range.

[17] Continuing the effort of *Liu et al.* [2005] on constructing simple solubility models, we make an effort to construct a simple H_2O solubility model in all natural or nearly natural (such as Fe free) silicate melts. It is necessary to choose compositional parameters to account for the dependence of H_2O solubility on melt composition. In previous models, *Moore et al.* [1998] employed mole fractions of Al_2O_3, FeO_t, and Na_2O, and *Behrens and Jantos* [2001] used a single compositional parameter of (2Mg + 2Ca + Li + Na + K − Al)/(total oxygen). After some trials, H_2O solubility appears to depend on the parameter AI = (Na + K − Al), where Na, K, and Al are cation mole fractions of the melt. All experimental H_2O solubility data in equilibrium with pure H_2O vapor used in the models of *Moore et al.* [1998], *Behrens and Jantos* [2001], and *Liu et al.* [2005] are combined (auxiliary material[1] Data Set S1) to derive the following simple model for H_2O solubility in natural silicate melts:

$$C_w = \left(-0.231 + \frac{651.1}{T}\right)\sqrt{P} + \left(0.03424 - \frac{32.57}{T} + 0.02447\mathrm{AI}\right)P, \quad (10)$$

where C_w is total H_2O solubility in weight percent, P is pressure in MPa, and T is temperature in kelvins. The applicable pressure range is 0–800 MPa (slightly larger than the range of applicability of equation (7), but equation (7) also works for gas mixtures), and the temperature range is 971–1623 K. The 2σ absolute error in predicting H_2O solubility is 0.68 wt %, and the 2σ relative error is 19%. Comparison between the fit and data is shown in Figure 4b. We recommend equation (10) for the calculation of H_2O solubility in all silicate melts in equilibrium with pure H_2O vapor. We have not yet arrived at a simple model for mixed CO_2-H_2O solubilities in all natural melts, whose full range would include carbonatite as well as silicate compositions.

[18] Even the best H_2O solubility model can only reproduce the experimental data to about 10% relative on average, meaning that the error in the calculated saturation pressure from a given H_2O_t content is of the order of 20%. The errors in solubility models largely arise from scatters in the experimentally determined solubility by various laboratories over the years. To improve the solubility models further, it is necessary to produce a set of highly accurate and internally consistent solubility data covering a wide range of temperature and pressure.

3. DIFFUSIVITY OF VOLATILES IN SILICATE MELTS

[19] In this section we review the diffusion of major volatile components in silicate melts, including H_2O, CO_2, and S. Ar diffusion is also discussed because it has applications to CO_2 diffusion as well as H_2O diffusion.

3.1. H_2O Diffusivity in Silicate Melts

3.1.1. H_2O Diffusivity in Rhyolitic Melts

[20] Many authors have investigated H_2O diffusion in rhyolitic melts. *Shaw* [1974] carried out the first experimental study on H_2O diffusion. At that time, there was no microanalytical technique to analyze the concentration profile of H_2O. *Shaw* [1974] measured the total mass gain during hydration of obsidian melt at high temperature and inferred the dependence of H_2O_t diffusivity on H_2O_t content. In retrospect, it is astonishing that the dependence inferred by *Shaw* [1974] was close to the most recent understanding [see *Zhang and Behrens*, 2000, Figure 9a]. *Jambon* [1979] determined the mass loss during dehydration to extract H_2O_t diffusivity, and some of his results were reexamined by *Jambon et al.* [1992]. *Delaney and Karsten* [1981] were the first to determine H_2O_t concentration profiles. They carried out hydration experiments, measured the H_2O_t concentration profile using an ion microprobe, and examined the concentration dependence of H_2O_t diffusivity. They inferred that H_2O_t diffusivity depends exponentially on H_2O_t concentration. Although the exponential relation for total H_2O diffusivity was thought to be an improvement over the results of *Shaw* [1974], later studies [*Zhang and Behrens*, 2000] show that the more complicated relation of *Shaw* [1974] is, in fact, more accurate, but the simple exponential form is applicable to molecular H_2O diffusion. *Karsten et al.* [1982] examined the temperature dependence of H_2O_t diffusivity using the same experimental and analytical technique as *Delaney and Karsten* [1981]. *Stanton et al.* [1985] found that diffusivities of H_2O and D_2O are similar, correcting an earlier claim from the same laboratory that the two differed significantly.

[21] The next major advance was the development of infrared spectroscopy, which allowed microanalytical determination of the concentration of H_2O_t and the two hydrous species, H_2O_m and OH [*Stolper*, 1982a, 1982b; *Newman et al.*, 1986]. *Zhang et al.* [1991a] carried out dehydration experiments of natural hydrous obsidian at relatively low

[1] Auxiliary materials are available at ftp://ftp.agu.org/apend/rg/2006rg000216.

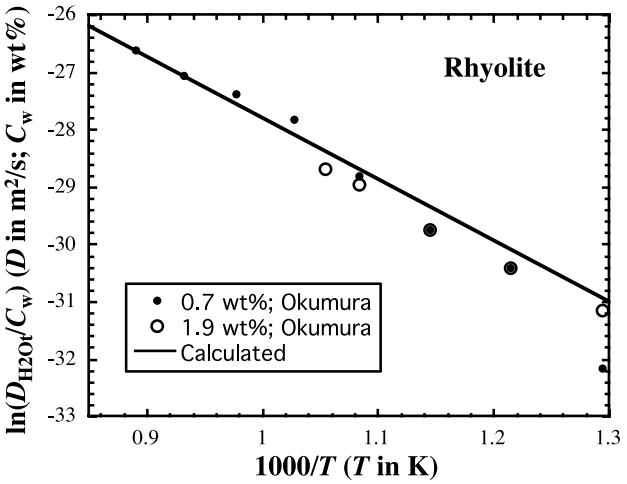

Figure 6. Experimental diffusion data (open and solid circles) of *Okumura and Nakashima* [2004] compared with calculated diffusivity (solid line) from equation (15). The diffusion-out diffusivities of *Okumura and Nakashima* [2004] have been divided by 0.347 to obtain $D_{H_2O_t}$ at the given H_2O_t [*Wang et al.*, 1996]. One point at 773 K and 0.7 wt % is lower than the predicted diffusivity because there is major disequilibrium between molecular H_2O and hydroxyl [cf. *Jambon et al.*, 1992].

temperatures (400°–550°C) and low H_2O_t ($\leq$1.8 wt %). After quenching they determined the concentration profiles of both H_2O_m and OH using the infrared spectroscopy. They carried out kinetic experiments to show that the species concentrations can be quenched without modification from such low temperatures. (Although there was debate about whether species concentrations can be quenched without modification from such intermediate temperatures [*Zhang et al.*, 1995; *Nowak and Behrens*, 1995; *Shen and Keppler*, 1995], the debate was resolved [*Withers et al.*, 1999] by the two debating sides with the conclusion that quenching from intermediate temperatures such as 673–873 K does maintain the species concentrations. That is, the claim that species reaction continues at 400–800 K based on in situ studies [*Nowak and Behrens*, 1995; *Shen and Keppler*, 1995] is invalid.) The concentration profiles of both H_2O_m and OH were fit by the solution to the following one-dimensional multispecies diffusion equation by varying diffusivity of OH and H_2O_m (each is assumed to be a constant) [*Zhang et al.*, 1991a, 1991b]:

$$\frac{\partial[H_2O_t]}{\partial t} = \frac{\partial}{\partial x}\left(D_{H_2O_m}\frac{\partial[H_2O_m]}{\partial x} + D_{OH}\frac{\partial[OH]/2}{\partial x}\right), \qquad (11)$$

where $D_{H_2O_m}$, and D_{OH} are the diffusivities of H_2O_m, and OH (and $D_{H_2O_t}$ will refer to the diffusivity of H_2O_t), brackets mean mole fractions on a single oxygen basis, and the mole fractions are related as $[H_2O_t] = [H_2O_m] + [OH]/2$ because two OH groups convert into one H_2O_m. Equation (11) is similar to Fick's second law of diffusion $\partial C/\partial t = \partial(D\partial C/\partial x)/\partial x$, but there are two terms (instead of one single term) on the right-hand side due to two species of H_2O: Each of the two terms accounts for the diffusion of a species. The fitting results of the experimental profiles show that $D_{OH} \ll D_{H_2O_m}$ and $D_{H_2O_m}$ is roughly constant for $H_2O_t \leq 1.8$ wt %. That is, for H_2O_t diffusion, H_2O_m is the mobile species and OH is basically immobile, which is consistent with the glass science literature on H_2O_t diffusion at very low H_2O_t ($\leq$0.1 wt %) [e.g., *Doremus*, 1969]. The result may be explained as follows: H_2O_m is a small neutral molecule that can move relatively easily, but OH is bonded to a cation and hence cannot move easily.

[22] *Nowak and Behrens* [1997] carried out the first diffusion couple experiments on haplogranitic melts with H_2O_t varying from 0.02 to 9.0 wt % at relatively high temperatures. They measured H_2O_t profiles and determined $D_{H_2O_t}$ using the Boltzmann-Matano method. From their data they pointed out that $D_{H_2O_m}$ could not be constant at H_2O_t content above 3.0 wt %. *Zhang and Behrens* [2000] carried out dehydration and diffusion couple experiments and combined the new data with previous data to construct a practical model for H_2O diffusivity applicable to H_2O_t from 0.1 to 7.7 wt %, temperature from 400°C to 1200°C, and pressure between 0.1 and 810 MPa (but the pressure effect is not well resolved). All the experimental data are consistent with (1) $D_{OH} \ll D_{H_2O_m}$ and (2) $D_{H_2O_m}$ increases exponentially with H_2O_t content:

$$D_{H_2O_m} = D_0 e^{\alpha X}, \qquad (12)$$

where X is the mole fraction of H_2O_t, D_0 is $D_{H_2O_m}$ at $X \to 0$, and α is a parameter characterizing how strongly $D_{H_2O_m}$ depends on H_2O_t. The larger the value of α (e.g., >20), the stronger is the dependence of $D_{H_2O_m}$ on H_2O_t. When α is small (e.g., $\leq$10, depending on maximum H_2O_t), H_2O_t diffusion profiles may be fit well using $D_{H_2O_t}$ proportional to H_2O_t [*Doremus*, 2004], but profiles with larger α values (such as Rhy-DC1, Rhy-DC4, Rhy-DC3, and KS&3-D16P given by *Zhang and Behrens* [2000]) require a more complicated function such as equation (12).

[23] The exponential dependence results in almost constant $D_{H_2O_m}$ at low H_2O_t and rapid increase of $D_{H_2O_m}$ at high H_2O_t. The assumption that $D_{H_2O_m}$ increases exponentially with H_2O_t is consistent with the diffusion behavior of CO_2 [*Watson*, 1991] and Ar [*Behrens and Zhang*, 2001]. *Okumura and Nakashima* [2004] dehydrated hydrous rhyolitic glass at intermediate temperatures, measured the loss of H_2O_t in situ by infrared spectroscopy, and obtained diffusion-out diffusivity, which is some average of the concentration-dependent diffusivity along the concentration profile [*Zhang et al.*, 1991a; *Wang et al.*, 1996; *Zhang*, 1999a]. The in situ measurement has the advantage of being simple and rapid, but it is difficult to determine the concentration dependence of diffusivity using the mass loss method. The data of *Okumura and Nakashima* [2004] are consistent with those of *Zhang and Behrens* [2000] (Figure 6).

[24] Currently, the best model to predict H_2O diffusivity in rhyolitic melt is that of *Zhang and Behrens* [2000] covering a wide temperature range (673–1473 K) and a wide range of H_2O_t (0.1–7.7 wt %) and with some limited pressure coverage from 0.1 to 810 MPa. The diffusivity of H_2O_m depends on T, P, and H_2O_t as follows:

$$\ln D_{H_2O_m} = \left(-13.55 - \frac{13128}{T} - 2.796\frac{P}{T}\right) + \left(-27.21 + \frac{36892}{T} + 57.23\frac{P}{T}\right)X, \quad (13)$$

where $D_{H_2O_m}$ is in $m^2\ s^{-1}$, T is in kelvins, P is in MPa, and X is the mole fraction of H_2O_t on a single oxygen basis. The diffusivity of H_2O_t (which is the diffusivity needed for modeling total H_2O diffusion profile and for calculating bubble growth rate) is related to $D_{H_2O_m}$ as follows:

$$D_{H_2O_t} = D_{H_2O_m}\frac{dX_m}{dX}, \quad (14)$$

where X_m is the mole fraction of H_2O_m on a single oxygen basis. The equilibrium relation between the differential dX_m/dX and H_2O_t is shown in Figure 2b. At low H_2O_t, $D_{H_2O_m}$ is roughly constant, and dX_m/dX is roughly proportional to H_2O_t, leading to proportionality between $D_{H_2O_t}$ and H_2O_t content. At high H_2O_t, $D_{H_2O_m}$ increases exponentially with H_2O_t, and dX_m/dX is roughly constant, leading to exponential increase of $D_{H_2O_t}$ with H_2O_t content.

[25] If equilibrium is not reached (e.g., low temperature such as 700 K and low H_2O_t such as 0.7 wt %), the differential in equation (14) depends on the kinetics of the reaction. For example, if molecular H_2O diffused away but is not replenished by reaction from OH, then dX_m/dX would be smaller than the equilibrium value, leading to smaller $D_{H_2O_t}$ [*Jambon et al.*, 1992].

[26] Although $D_{H_2O_t}$ can be calculated from equations (13) and (14), the procedure of calculation is a little complicated because the differential dX_m/dX takes some effort to calculate. For ease of application, *Zhang and Behrens* [2000] obtained explicit expressions of $D_{H_2O_t}$. For $H_2O_t \le 2$ wt % the expression of $D_{H_2O_t}$ is simple:

$$\ln\frac{D_{H_2O_t}}{C_w} = -17.14 - \frac{10661}{T} - 1.772\frac{P}{T}, \quad (15)$$

where $D_{H_2O_t}$ is in $m^2\ s^{-1}$, C_w is H_2O_t in weight percent, P is in MPa, and T is in kelvins. The accuracy of the formula is better than a factor of 2 at 673–1473 K, $H_2O_t \le 2$ wt %, and 0.1–810 MPa. For example, Figure 6 compares the recent experimental data of *Okumura and Nakashima* [2004] at $H_2O_t \le 2$ wt % with equation (15), and the agreement is excellent (within 0.4 in terms of ln$D$) except for one point at 773 K and 0.7 wt % H_2O_t. The exception is due to the slow reaction rate governing the regeneration of molecular H_2O at such low temperature and H_2O_t [*Jambon et al.*, 1992].

[27] The equation for calculating $D_{H_2O_t}$ at all conditions covered by *Zhang and Behrens* [2000] is

$$D_{H_2O_t} = 10^{-12}X\exp(m)\left\{1+\exp\left[56+m+X\left(-34.1.+\frac{44620}{T}+\frac{57.3P}{T}\right)-\sqrt{X}\left(0.091+\frac{4.77\times10^6}{T^2}\right)\right]\right\}, \quad (16)$$

where $D_{H_2O_t}$ is in $m^2\ s^{-1}$, $m = -20.79 - 5030/T - 1.4P/T$, P is in MPa, and T is in kelvins. Note that in the work of *Zhang and Behrens* [2000] the equation in the abstract is correct, but equation (14) in their text contains a typographical error, in which 5.73 should be 57.3. *Zhang and Behrens* [2000] pointed out, and *Behrens et al.* [2007] corroborated, that the pressure dependence of $D_{H_2O_t}$ needs to be better constrained. Recently, *Behrens et al.* [2007] confirmed that molecular H_2O is the carrier for oxygen diffusion in rhyolitic melt [*Zhang et al.*, 1991b]. It is hoped that these equations will be improved further in the near future with more data on the pressure dependence of H_2O diffusion.

[28] Among the equations for diffusivity the temperature and pressure dependences are theoretical (Arrhenius equation and transition state theory), although the coefficients (activation energy and activation volume) are experimentally derived. The dependence of $D_{H_2O_m}$ on H_2O content (equation (12)) is empirical [*Zhang and Behrens*, 2000] and is consistent with other experimental data on CO_2 and Ar diffusion; no theory is available on how diffusivity depends on composition. The dependences of $D_{H_2O_t}$ on T, P, and H_2O content (equations (15) and (16)) are based on the theoretical relation between $D_{H_2O_t}$ and $D_{H_2O_m}$ (equation (14)) and some empirical considerations.

3.1.2. H_2O Diffusivity in Other Natural Melts

[29] H_2O diffusion in other natural melts has not been investigated as extensively as that in rhyolitic melt. Glass scientists investigated H_2O diffusion in various commercial glasses [e.g., *Drury and Roberts*, 1963; *Cockram et al.*, 1969; *Doremus*, 1969; *Burn and Roberts*, 1970; *Lanford et al.*, 1979; *Houser et al.*, 1980; *Tsong et al.*, 1980; *Nogami and Tomozawa*, 1984; *Tomozawa*, 1985; *Oehler and Tomozawa*, 2004], but only the work on natural melts (including synthetic melts that approximate natural melts) will be reviewed below. Some of the melt compositions that have been investigated for H_2O diffusion are listed as compositions 1–10 in Table 1 on the anhydrous basis. *Zhang and Stolper* [1991] reported data on H_2O diffusion in basalt at 1 GPa, 1573–1773 K, and $H_2O_t < 0.5$ wt %. *Freda et al.* [2003] carried out experiments on H_2O diffusion in a potassium-rich trachyte at 1 GPa, 1373–1673 K, and $H_2O_t < 2$ wt %. *Liu et al.* [2004] studied H_2O diffusion in dacitic melt at <150 MPa, 824–910 K, and $H_2O_t < 2.5$ wt %. *Behrens et al.* [2004] investigated H_2O diffusion in dacitic and andesitic melts at 0.5–1.5 GPa, 1458–1858 K, and H_2O_t

TABLE 1. Chemical Composition for H_2O and CO_2 Diffusion Studies[a]

ID	Composition	SiO_2	TiO_2	Al_2O_3	FeO	MnO	MgO	CaO	Na_2O	K_2O	P_2O_5	Ref[b]
1	rhyolite 1	76.59	0.08	12.67	1.00	0.00	0.03	0.52	3.98	4.88		1,2
2	AOQ	76.14	0	11.53	0	0	0	0	4.65	5.68		3
3	rhyolite 2	77.3	0.1	13.0	0.5	0.0	0.1	0.5	3.8	4.7		4
4	dacite 1	65.03	0.67	16.63	4.16		1.96	5.10	3.95	2.70		5,6
5	dacite 3	67.54	0.77	15.74	4.28	0.12	1.43	4.40	3.58	2.15		7
6	andesite 1	57.21	0.84	17.50	7.58	0.11	4.27	7.59	3.31	1.60		6
7	andesite 2	62.54	0.70	16.74	5.55	0.10	2.97	6.48	3.20	1.69		7
8	trachyte	59.9	0.39	18.0	0.89	0.12	3.86	2.92	4.05	8.35	0.21	8
9	basalt 1	50.6	1.88	13.9	12.5	0.23	6.56	11.4	2.64	0.17	0.21	9
10	basalt 2	46.12	1.50	16.11	10.84	0.20	7.60	13.32	3.56	0.76		7
11	synthetic	60		10					30			10
12	haplobasalt	52.9	2.1	13.2			16.6	10.6	3.0	1.1	0.5	10
13	rhyolite	76.45	0.08	12.56	1.02	0.08	0.06	0.25	4.21	4.78		11
14	rhyolite	77.5	0.07	13.0	0.56	0.04	0.05	0.52	4.10	4.18		13
15	rhyolite	76.4	0.15	13.35	0.79	0.06	0.07	0.51	4.31	4.67		12
16	dacite	63.5	0.56	17.61	4.91		1.68	5.24	4.67	1.77		12
17	basalt	50.6	1.88	13.9	12.5	0.23	6.56	11.4	2.64	0.17		14

[a]Compositions are listed on the anhydrous basis. Compositions 11–17 are for CO_2 diffusion experiments. Composition 11 is a sodium aluminosilicate. Compositions are given in weight percent.

[b]References are as follows: 1, *Zhang et al.* [1991a]; 2, *Zhang and Behrens* [2000]; 3, *Nowak and Behrens* [1997]; 4, *Okumura and Nakashima* [2004]; 5, *Liu et al.* [2004]; 6, *Behrens et al.* [2004]; 7, *Okumura and Nakashima* [2006]; 8, *Freda et al.* [2003]; 9, *Zhang and Stolper* [1991]; 10, *Watson et al.* [1982]; 11, *Fogel and Rutherford* [1990]; 12, *Watson* [1991]; 13, *Blank* [1993]; and 14, *Zhang and Stolper* [1991].

$\leq$ 6.3 wt %. *Okumura and Nakashima* [2006] conducted dehydration experiments with in situ infrared measurement to extract the diffusion-out diffusivity of H_2O_t in basaltic, andesitic, and dacitic glasses at 0.1 MPa, 673–948 K, and $H_2O_t \leq 1.1$ wt %. Almost every paper examined a different melt or a different *P-T* range except for the in situ study of *Okumura and Nakashima* [2006], who reproduced some of the previous results. Therefore their results provide a check of data consistency among different laboratories. For example, $D_{H_2O_t}$ data in dacite reported by *Okumura and Nakashima* [2006] are consistent with those reported by *Liu et al.* [2004] within 0.6 units in terms of ln*D* (Figure 7a), which is a typical interlaboratory data precision.

[30] There are not enough experimental data to produce a general model to predict H_2O diffusivity in all natural silicate melts. Sections 3.1.2.1–3.1.2.5 are a summary of H_2O diffusion in different natural melts.

3.1.2.1. Dacitic Melt

[31] H_2O diffusion in dacitic melt has been investigated in two *T-P* regions in three studies: Two were conducted at intermediate temperature (773–948 K) and low pressure (<150 MPa) with $H_2O_t < 2.5$ wt % [*Liu et al.*, 2004; *Okumura and Nakashima*, 2006], and one was conducted at high temperature (1458–1798 K) and high pressure (0.5–1.5 GPa) with H_2O_t between 0.1 and 6.3 wt % [*Behrens et al.*, 2004]. Data in the concentration range where $D_{H_2O_t}$ is proportional to H_2O_t ($H_2O_t \leq 0.8$ wt % at 773–948 K [*Liu et al.*, 2004] and $H_2O_t \leq 6.3$ wt % at 1458–1798 K [*Behrens et al.*, 2004]) are shown in Figure 7a. At 773–948 K, $D_{H_2O_t}$ increases more rapidly with H_2O_t than simple proportionality at $H_2O_t > 0.8$ wt %, which can be modeled well by assuming D_{OH} is negligible and $D_{H_2O_m}$ increases exponentially with H_2O_t content [*Liu et al.*, 2004], as is the case for rhyolitic melt. If we only consider the H_2O_t range in which $D_{H_2O_t}$ is proportional to H_2O_t and ignore the pressure dependence, all the experimental data on dacitic melt may be fit to obtain the following (Figure 7a):

$$\ln \frac{D_{H_2O_t}}{C_w} = -14.66 - \frac{15086}{T}, \quad (17)$$

where $D_{H_2O_t}$ is in $m^2\ s^{-1}$, C_w is in weight percent, T is in kelvins, and the coefficient of determination $r^2 = 0.9962$. (The fits to diffusion profile or to the diffusion data often show high values of r^2. Experience shows that at such high values of r^2, visual examination of the data and fit is the best way to evaluate the quality of the fit.) The above equation is applicable to $H_2O_t \leq 0.8$ wt % at 800 K and to $H_2O_t \leq 6$ wt % at 1600 K. We estimate that the error is about a factor of 3 in terms of *D* in the applicable range (the estimated error is larger than fitting error in Figure 7a because the pressure effect is not considered in the fit). It is necessary to investigate H_2O diffusion at intermediate temperatures (about 800 K) and high pressures (0.5–1.5 GPa) to constrain the pressure dependence of $D_{H_2O_t}$.

3.1.2.2. Basaltic Melt

[32] H_2O diffusion in basaltic melt has been investigated in two *T-P* regions in two studies: dehydration experiments at 673–848 K and 0.1 MPa with initial $H_2O_t = 1.1$ wt % [*Okumura and Nakashima*, 2006] and diffusion couple experiments at 1573–1773 K and 1 GPa with $H_2O_t <$ 0.45 wt % [*Zhang and Stolper*, 1991]. The data are shown in Figure 7d. *Zhang and Stolper* [1991] found that the H_2O diffusion profile can be fit well by assuming $D_{H_2O_t}$ is proportional to H_2O_t. *Okumura and Nakashima* [2006] obtained diffusivity from mass loss data, which cannot reveal how $D_{H_2O_t}$ depends on H_2O_t. By assuming $D_{H_2O_t}$ is proportional to H_2O_t, the two diffusion data sets are consistent with a negligible or small pressure effect. Ignor-

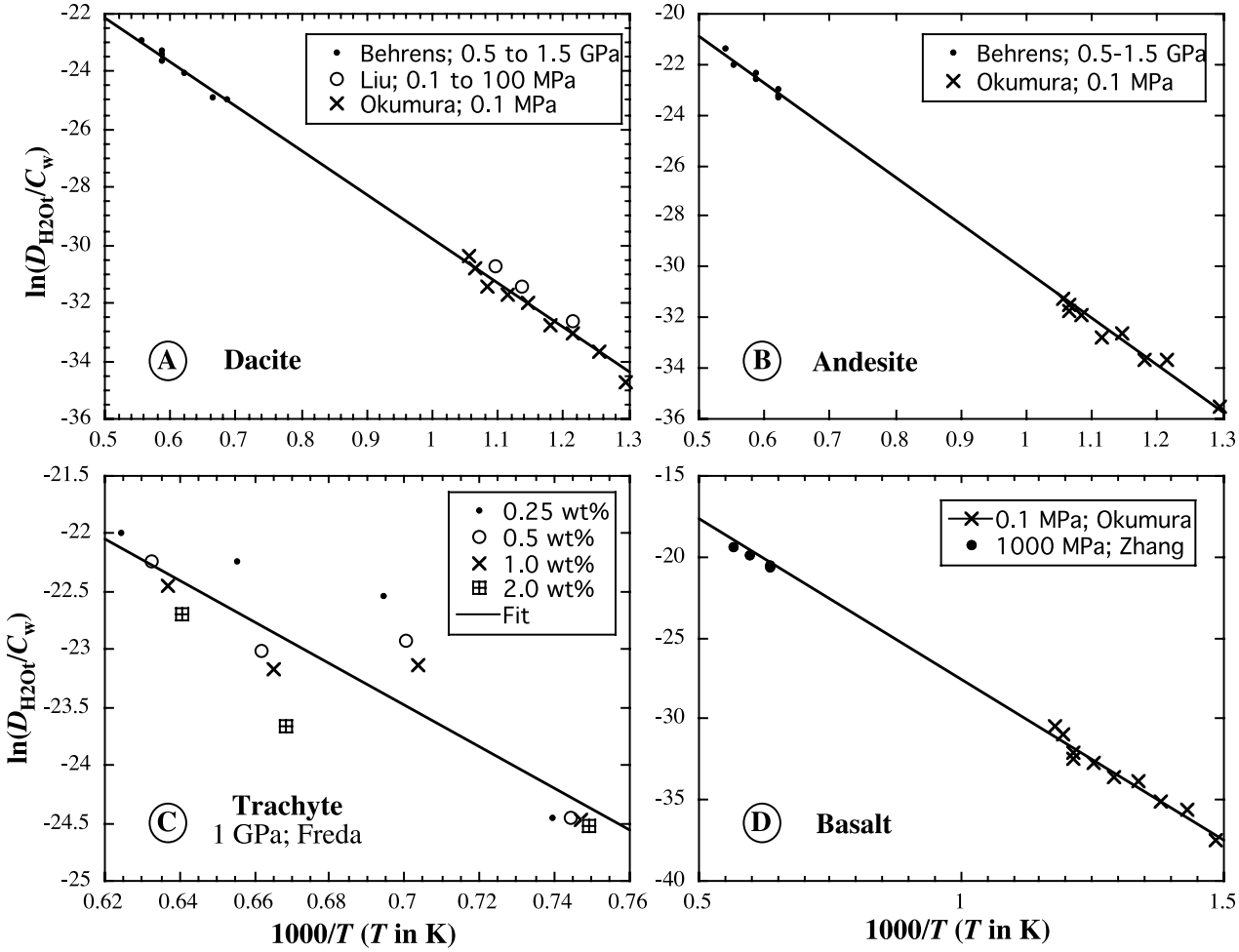

Figure 7. Experimental H_2O diffusivity data in four different melts: (a) dacite, (b) andesite, (c) trachyte, and (d) basalt. The vertical axis is $\ln(D/C_w)$, where D is H_2O_t diffusivity in $m^2\ s^{-1}$ and C_w is H_2O_t in weight percent. Three melts (dacite, andesite, and basalt) have been investigated by two or more groups, and the high-temperature and low-temperature data are roughly consistent. Data sources are *Zhang and Stolper* [1991], *Freda et al.* [2003], *Behrens et al.* [2004], *Liu et al.* [2004], and *Okumura and Nakashima* [2006].

ing the pressure effect, the data are well described by the following equation (Figure 7d):

$$\ln\frac{D_{H_2O_t}}{C_w} = -8.56 - \frac{19110}{T}. \quad (18)$$

[33] The coefficient of determination is $r^2 = 0.9964$. Equation (18) is applicable to $H_2O_t \leq 1.1$ wt % at about 800 K and is expected to be applicable to greater H_2O_t at higher temperatures. The accuracy is estimated to be about a factor of 3 in terms of D in the applicable range. It is necessary to investigate H_2O diffusion at intermediate temperatures (about 800 K) and high pressures (0.5–1.5 GPa) to constrain the pressure dependence of $D_{H_2O_t}$. It is also necessary to examine H_2O_t diffusion at high H_2O_t.

3.1.2.3. Andesitic Melt

[34] H_2O diffusion in andesitic melt has been investigated in two studies, at 1558–1848 K and 0.5 and 1 GPa with $H_2O_t \leq 5.6$ wt % [*Behrens et al.*, 2004] and at 773–948 K and 0.1 MPa with $H_2O_t \leq 0.7$ wt % [*Okumura and Nakashima*, 2006]. Curiously, in andesitic melt at 1558–1848 K, $D_{H_2O_t}$ is almost independent of H_2O_t [*Behrens et al.*, 2004]. At intermediate temperatures, only the diffusion-out diffusivities have been obtained [*Okumura and Nakashima*, 2006], which cannot constrain how $D_{H_2O_t}$ depends on H_2O_t. Because we do not understand why $D_{H_2O_t}$ in andesite is almost independent of H_2O_t, for consistency and following *Behrens et al.* [2004], we still treat $D_{H_2O_t}$ in andesite to be proportional to H_2O_t. Ignoring the pressure dependence of $D_{H_2O_t}$, then two data sets may be fit by the following (Figure 7b):

$$\ln\frac{D_{H_2O_t}}{C_w} = -11.63 - \frac{18582}{T}. \quad (19)$$

[35] The coefficient of determination is $r^2 = 0.9990$. The accuracy of equation (19) is estimated to be about a factor of

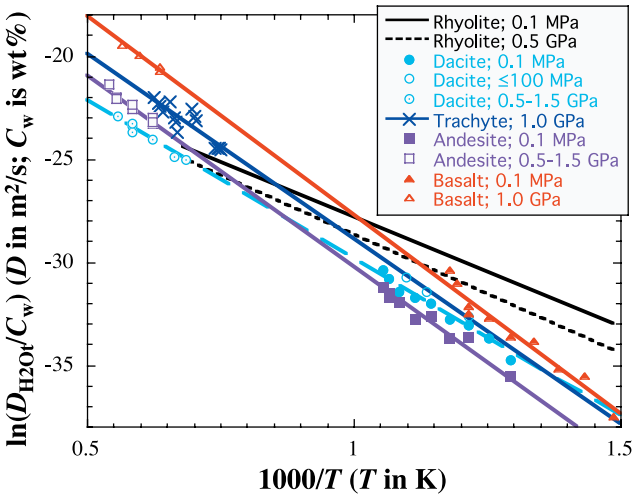

Figure 8. Comparison of experimental H_2O diffusion data under various conditions in the concentration range where D is assumed to be proportional to C. For rhyolite, only the calculated lines are given for 0.1 MPa (black solid line) and 0.5 GPa (black dashed line). Even for rhyolite the pressure effect is not well known. For other melts, there are not enough data to resolve the pressure effect, and hence the pressure effect is ignored. Red indicates data and fit for basalt; sky blue indicates dacite; purple indicates andesite; and blue indicates trachyte. Reference for dacite (0.5–1.5 GPa) is *Behrens et al.* [2004], for dacite (<0.1 GPa) is *Liu et al.* [2004], and for dacite (0.0001 GPa) is *Okumura and Nakashima* [2006]. Reference for basalt (1 GPa) is *Zhang and Stolper* [1991] and for basalt (0.0001 GPa) is *Okumura and Nakashima* [2006]. Reference for andesite (0.5–1.5 GPa) is *Behrens et al.* [2004] and for andesite (0.0001 GPa) is *Okumura and Nakashima* [2006]. Reference for trachyte (1 GPa) is *Freda et al.* [2003]. Data of *Liu et al.* [2004] with H_2O_t > 1.0 wt % are not included because at such low temperatures, $D_{H_2O_t}$ is proportional to C only to about 1.0 wt % H_2O_t. The diffusion-out diffusivities of H_2O_t [*Okumura and Nakashima*, 2006] have been divided by 0.347 to obtain $D_{H_2O_t}$ at the maximum H_2O_t along the profile.

3 in terms of D for $H_2O_t \leq 2$ wt % even though the reproducibility is better.

3.1.2.4. Trachytic Melt

[36] H_2O diffusion in trachytic melt has been investigated in only one paper at 1373–1673 K and 1 GPa with H_2O_t < 2 wt % [*Freda et al.*, 2003]. $D_{H_2O_t}$ values were obtained by the Boltzmann-Matano method. The data seem to indicate that $D_{H_2O_t}$ is proportional to H_2O_t at about 1340 K, but it is not so at higher temperatures. Because detailed information is not available for more careful assessment, for consistency we assume that $D_{H_2O_t}$ is proportional to H_2O_t. Then the data may be fit to obtain (Figure 7c):

$$\ln\frac{D_{H_2O_t}}{C_w} = -10.90 - \frac{17975}{T}. \quad (20)$$

[37] The coefficient of determination is $r^2 = 0.7945$. Equation (20) reproduces experimental data to within 0.8 units in terms of ln$D$. Because the temperature range covered by the experiments is small (1373–1673 K), extrapolation of equation (20) to lower or higher temperatures is not recommended.

3.1.2.5. All Melts

[38] Figure 8 compares H_2O diffusivity in different melts. At high temperatures (>1100 K), $D_{H_2O_t}$ increases from polymerized rhyolite to depolymerized basalt. At lower temperatures, there is no consistent trend. Equations (15) and (17)–(20), applicable to low H_2O_t (the applicable H_2O_t range depends on the melt and temperature), are in the form of $\ln(D/C_w) = A - B/T$, where A and B are fitting parameters in equations (17)–(20). Although it is an oversimplification to characterize each melt merely by the SiO_2 content, Figure 9 shows that A is almost linearly correlated with SiO_2 and B (proportional to the activation energy for diffusion) is a nonlinear function of SiO_2. That is, there is systematic relation between H_2O diffusivity and melt composition (mostly SiO_2 concentration). It is therefore hoped that a systematic understanding of H_2O diffusivity in natural melts will be achieved in the near future with more H_2O diffusivity data.

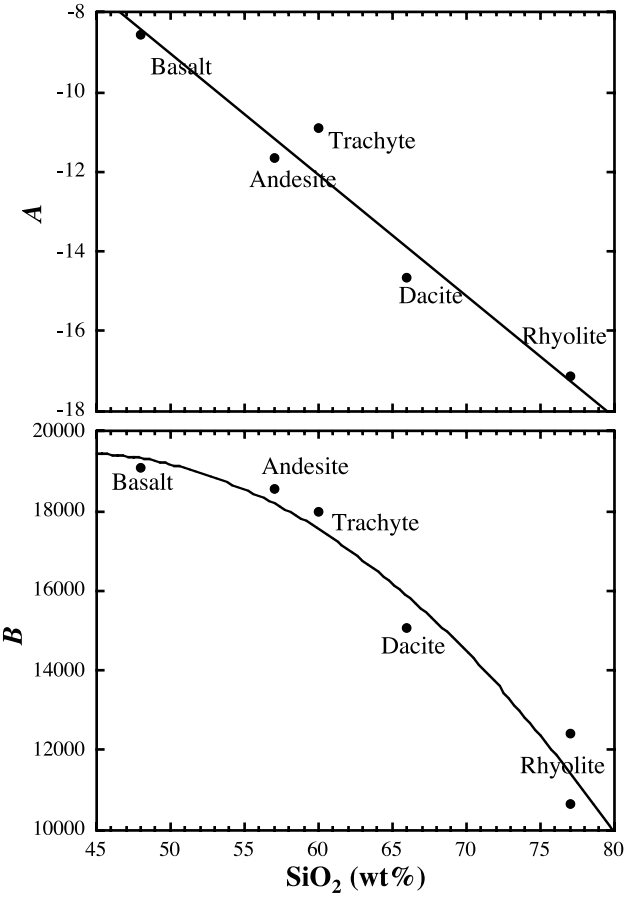

Figure 9. Parameters A and B versus SiO_2 content. The parameters A and B are fitting parameters in $\ln(D_{H_2O_t}/C_w) = A - B/T$, where $D_{H_2O_t}$ is in $m^2\ s^{-1}$, C_w is H_2O_t content in weight percent, and T is temperature in kelvins.

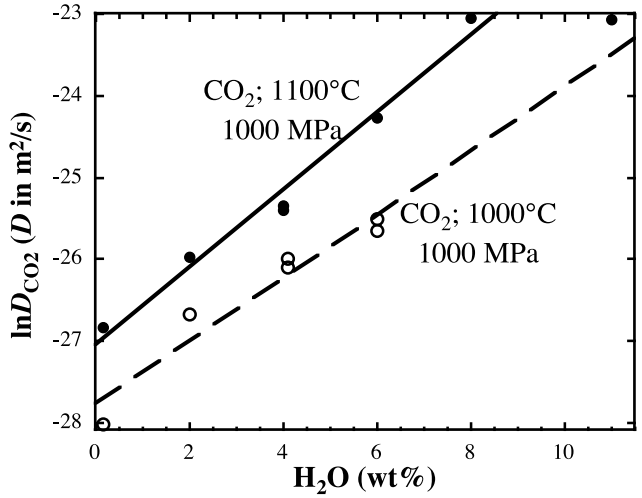

Figure 10. CO_2 diffusivity as a function of H_2O_t content at two different temperatures: 1100°C (solid circles and solid line) and 1000°C (open circles and dashed line). Data are from *Watson* [1991].

3.2. CO_2 Diffusivity in Silicate Melts

[39] CO_2 is usually the second most abundant volatile component in natural silicate melts. Because of its much smaller solubility, CO_2 often contributes more to the gas phase. Hence understanding its diffusivity (and solubility) is critical to the understanding of degassing especially for basaltic melt.

[40] As is the case for H_2O, a dissolved CO_2 component may be present in silicate melts as at least two species: CO_2 molecules and CO_3^{2-} groups. For clarity, hereinafter CO_2 refers to the component, molecular CO_2 or $CO_{2,molec}$ refers to the molecular species, CO_3^{2-} refers to the carbonate species, and $CO_{2,total}$ refers to the total content. The speciation reaction may be written as follows:

$$CO_{2,molec}(melt) + O^{2-}(melt) \rightleftharpoons CO_3^{2-}(melt), \qquad (21)$$

where O^{2-} is a free oxygen anion in the melt. The equilibrium constant denoted as K_{22} is

$$K_{22} = \frac{[CO_3^{2-}]}{[CO_{2,molec}][O^{2-}]}, \qquad (22)$$

where brackets mean activities approximated by mole fractions. For a given melt, $[O^{2-}]$ is fixed. Hence $[CO_3^{2-}]$ is proportional to $[CO_2]$, unlike the case of H_2O component, in which the square of [OH] is proportional $[H_2O_m]$. The simple proportionality means that as total CO_2 concentration varies, $CO_{2,molec}/CO_{2,total}$ and $CO_3^{2-}/CO_{2,total}$ are roughly constant. Therefore, in contrast of dissolved H_2O in silicate melts in which the species concentration ratio depends strongly on its own concentration, CO_2 species concentration ratio does not depend on its own concentration but depends on the melt composition. In rhyolitic melt, CO_2 is mostly present as $CO_{2,molec}$. In basaltic melt, CO_2 is mostly present as CO_3^{2-}.

[41] Diffusion of CO_2 component in a number of silicate melts has been investigated by *Watson et al.* [1982], *Watson* [1991], *Blank* [1993], *Sierralta et al.* [2002], and *Nowak et al.* [2004]. *Fogel and Rutherford* [1990] and *Zhang and Stolper* [1991] also obtained some limited data on CO_2 diffusivity. *Watson et al.* [1982] carried out the first study of CO_2 diffusion using the thin-film method by depositing sodium carbonate (with ^{14}C) film on the surface of a sodium aluminosilicate glass or an iron-free "basalt" at 1073–1773 K and 50–1800 MPa. They made the surprising discovery that the diffusivity does not depend on the anhydrous melt composition from a haplobasaltic melt to a synthetic peralkaline melt containing 30% Na_2O. In order to understand the effect of dissolved H_2O on CO_2 diffusivity in silicate melts, *Watson* [1991] measured ^{14}C tracer diffusivity in hydrous rhyolitic and dacitic melts at 1073–1373 K, 1 GPa, and 0.15–11 wt % H_2O_t. He found that CO_2 tracer diffusivity depends exponentially on H_2O content (Figure 10) up to 8 wt % H_2O_t. Above 8 wt % H_2O_t, CO_2 tracer diffusivity seems to become independent of H_2O_t (Figure 10), which may be real or may be an experimental artifact. In the discussion below, H_2O_t concentration is limited to $\leq$8 wt % to avoid addressing the issue. *Blank* [1993] conducted CO_2 sorption experiments into anhydrous rhyolitic melt and determined CO_2 diffusivity in rhyolite at 723–1323 K and 50–105 MPa. She concluded that the effective binary diffusivity values are not much different from the tracer diffusivities of *Watson et al.* [1982] and *Watson* [1991]. *Sierralta et al.* [2002] investigated CO_2 diffusion in albite melt with 0–6.83 wt % additional Na_2O or 0–2 wt % H_2O_t at 1523 K and 500 MPa using the diffusion couple method. They found a small but systematic increase of CO_2 effective binary diffusivity with increasing H_2O and Na_2O. *Nowak et al.* [2004] further examined the dependence of CO_2 diffusivity on anhydrous melt composition by varying the melt composition from basalt to rhyolite using the diffusion couple method at 1623 K and 1 GPa. The compositional effect was found to be negligible. In addition, *Fogel and Rutherford* [1990] obtained three points of CO_2 diffusivity in a rhyolite as a byproduct of CO_2 solubility experiments, and *Zhang and Stolper* [1991] obtained one datum of CO_2 diffusivity in a Juan de Fuca basalt at 1573 K, 1 GPa, and 0.10 wt % H_2O_t as a by-product of H_2O diffusion. Some melt compositions that have been investigated for CO_2 diffusion are listed as compositions 11–17 in Table 1 on an anhydrous basis, and diffusion data are summarized in auxiliary material Data Set S2.

[42] The compositional range of the silicate melts investigated for carbon diffusion is large (compositions 11–17 in Table 1, plus compositions studied by *Sierralta et al.* [2002] and *Nowak et al.* [2004]). The speciation of CO_2 varies from $CO_{2,molec}$ to CO_3^{2-}. Total CO_2 diffusivity may be written as

$$D_{CO_{2,total}} = D_{CO_{2,molec}} \frac{dX_{CO_{2,molec}}}{dX_{CO_{2,total}}} + D_{CO_3^{2-}} \frac{dX_{CO_3^{2-}}}{dX_{CO_{2,total}}}. \qquad (23)$$

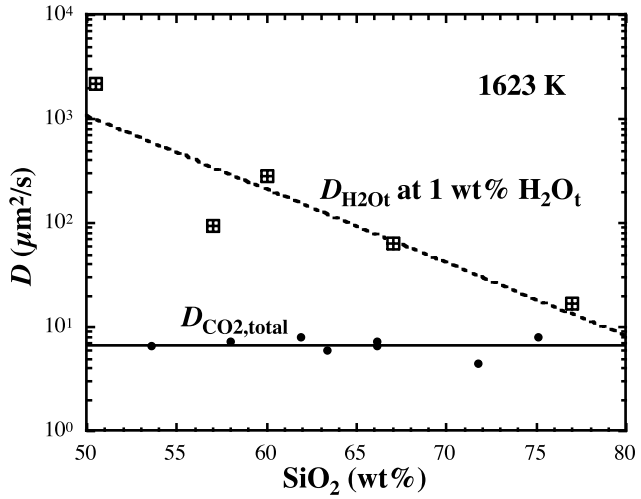

Figure 11. Comparison of $D_{H_2O_t}$ and $D_{CO_{2,total}}$ as a function of anhydrous melt composition. $D_{CO_{2,total}}$ is roughly independent of SiO_2 concentration, whereas $D_{H_2O_t}$ decreases with increasing SiO_2 content. There are scatters beyond the experimental uncertainty because the variations in melt composition cannot be simply described by SiO_2 concentration variation alone. Diffusivity data for CO_2 are from *Nowak et al.* [2004], and data for H_2O are from *Zhang and Behrens* [2000], *Freda et al.* [2003], *Behrens et al.* [2004], and *Liu et al.* [2004].

[43] Because both $dX_{CO_{2,molec}}/dX_{CO_{2,total}}$ and $dX_{CO_3^{2-}}/dX_{CO_{2,total}}$ are independent of total CO_2 concentration in a given melt, $CO_{2,total}$ diffusivity is not expected to depend on $CO_{2,total}$ concentration. That is, although speciation in the case of H_2O component leads to strong dependence of H_2O_t diffusivity on H_2O_t content, speciation in the case of the CO_2 component is not expected to lead to such dependence. Hence it is not surprising that experimental data on CO_2 diffusion can be fit well with concentration-independent D. The difference in the behavior of CO_2 and H_2O arises because in the speciation reaction of H_2O the stoichiometric coefficients for all hydrous species are not equal, but in the speciation reaction of CO_2, the stoichiometric coefficients for all carbon species are equal.

[44] Surprisingly, the diffusivities of total CO_2 do not even significantly depend on the anhydrous melt composition. CO_2 is the only component known to exhibit such independence. Figure 11 shows the near constancy of CO_2 diffusivity in various "dry" melts (H_2O_t content <0.3 wt %) in contrast with strong dependence of H_2O diffusivity on SiO_2. The observation may be explained as follows. Assuming the diffusing species is $CO_{2,molec}$ (which is reasonable because molecular CO_2 is neutral and smaller, whereas CO_3^{2-} is charged and larger), the diffusivity of total CO_2 (equation (23)) may be written as

$$D_{CO_{2,total}} = D_{CO_{2,molec}} \frac{dX_{CO_{2,molec}}}{dX_{CO_{2,total}}} = \frac{D_{CO_{2,molec}}}{1 + K_{22} X_{O^{2-}}}. \quad (24)$$

[45] It is expected that $D_{CO_{2,molec}}$ increases from rhyolite to basalt, leading to an increase of $D_{CO_{2,total}}$. On the other hand, the concentration of free oxygen ion O^{2-} also increases from rhyolite to basalt, leading to a decrease of $D_{CO_{2,total}}$. That is, in rhyolite, molecular CO_2 diffusivity is small, but its proportion is basically 100% (there is no detectable CO_3^{2-} in rhyolite), whereas in basalt, molecular CO_2 diffusivity is expected to be large but its proportion is small (there is no detectable molecular CO_2 in basalt). *Nowak et al.* [2004] suggested that the two factors roughly compensate each other and coincidentally make $D_{CO_{2,total}}$ roughly independent of anhydrous melt composition.

[46] The diffusion behaviors of both H_2O and CO_2 demonstrate the importance of understanding the role of speciation in diffusion and the very different consequences due to the role. For a component that is present as only one species (such as Ar), the diffusivity is expected to be independent of its own concentration if the concentration is low but dependent on the major oxide concentrations of the melt. H_2O is present as at least two species in silicate melts, and the effect of speciation leads to strong dependence of H_2O_t diffusivity on its own concentration. The diffusivity also depends on the anhydrous melt composition, as is the case of the one-species component. CO_2 is also present as at least two species in silicate melts, but speciation does not lead to concentration dependence of $CO_{2,total}$ diffusivity. Moreover, the speciation leads to $CO_{2,total}$ diffusivity being independent of the anhydrous melt composition. The two examples of H_2O and CO_2 diffusion demonstrate the richness of the effect of speciation on diffusion.

[47] The weak dependence of CO_2 diffusivity on melt composition is a blessing in simplifying the task of obtaining a general approximate expression for CO_2 diffusivity. Hence CO_2 may be the first component whose diffusivity may be predicted in all natural silicate melts. Because the diffusivities of total CO_2 do not significantly depend on the melt composition nor on carbon speciation, Figure 12 compares CO_2 diffusivity in various "dry" melts (H_2O_t content < 0.3 wt %), showing a general consistency of data for different melts and from different laboratories. Figure 12a shows in detail that the tracer diffusivity data (in red) of *Watson et al.* [1982] and *Watson* [1991] are highly self-consistent and that the chemical diffusivity or effective binary diffusivity data (in black) of *Fogel and Rutherford* [1990], *Zhang and Stolper* [1991], *Blank* [1993], *Sierralta et al.* [2002], and *Nowak et al.* [2004] are consistent, but the tracer diffusivities are slightly different from the effective binary diffusivities. For example, the tracer diffusivities show a significant pressure effect, but the effective binary diffusivities do not. Furthermore, at 500–600 MPa, tracer diffusivity (red solid circles) is significantly greater than the effective binary diffusivity (black open circles and squares) (Figure 12b). We tentatively attribute the difference to that between tracer and effective binary diffusivity, although the explanation is not entirely satisfactory because CO_2 concentrations in the effective binary diffusion experiments are also low (<0.23 wt %) and

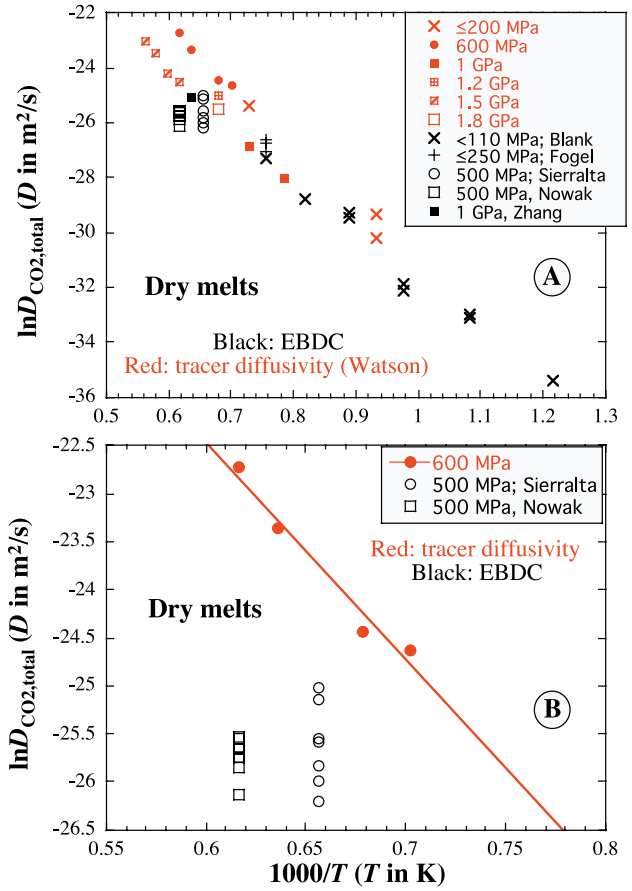

Figure 12. Diffusion data of CO_2 in anhydrous melts ($H_2O_t < 0.3$ wt %): (a) all data and (b) data at 500–600 MPa to highlight the differences in data. Tracer diffusivity data are indicated in red and are from *Watson et al.* [1982] and *Watson* [1991]. Chemical (or effective binary) diffusivity data are indicated in black and are from *Blank et al.* [1993], *Fogel and Rutherford* [1990], *Sierralta et al.* [2002], *Nowak et al.* [2004], and *Zhang and Stolper* [1991].

because there are no other major concentration gradients in the effective binary diffusion experiments.

[48] Below we attempt to construct an equation to predict CO_2 diffusivity. By ignoring the weak compositional effect the task is simplified, but it is necessary to tolerate slightly larger errors than normal experimental uncertainties (about a factor of 2 in terms of D or 0.7 in terms of ln$D$).

[49] Because experimental data show that $D_{CO_{2,total}}$ is an exponential function of H_2O_t content for $H_2O_t \leq 8$ wt % (Figure 10), we let

$$\ln D_{CO_{2,total}} = \ln D_0 + \alpha C_w, \tag{25}$$

where α is a constant at a given T and P, C_w is H_2O_t content, and D_0 is total CO_2 diffusivity in dry melt. Because lnD_0 may be modeled as $(a_0 + b_0/T + c_0P/T)$ and α can be modeled as $(a_1 + b_1/T + c_1P/T)$ [*Zhang and Behrens*, 2000], it is tempting to model $D_{CO_{2,total}}$ as follows (similar to equation (13)):

$$\ln D_{CO_{2,total}} = \left(a_0 + \frac{b_0}{T} + c_0\frac{P}{T}\right) + \left(a_1 + \frac{b_1}{T} + c_1\frac{P}{T}\right)C_w. \tag{26}$$

[50] However, examination of CO_2 diffusion data shows that the term c_1C_wP/T cannot be constrained because most high H_2O concentration experiments are conducted only at a single pressure of 1 GPa. Therefore the following equation is used to fit the data:

$$\ln D_{CO_{2,total}} = \left(a_0 + \frac{b_0}{T} + c_0\frac{P}{T}\right) + \left(a_1 + \frac{b_1}{T}\right)C_w. \tag{27}$$

[51] If all experimental data on CO_2 diffusion (including tracer and effective binary diffusivities) are used, then the following equation is the best fit to the 61 data points (excluding the two data points with 11 wt % H_2O_t):

$$\ln D_{CO_{2,total}} = -14.34 - \frac{17360 - 0.6527P}{T} + \left(-0.7172 + \frac{1436.8}{T}\right)C_w, \tag{28}$$

where $D_{CO_{2,total}}$ is CO_2 diffusivity in $m^2\ s^{-1}$, P is in MPa, T is in kelvins, and C_w is weight percent of H_2O_t. Equation (28) has a 2σ uncertainty of 1.44 in terms of lnD_{CO_2} (Figure 13a). The somewhat larger 2σ uncertainty than usual is because the difference between tracer diffusivity and effective binary diffusivity is ignored. Another strategy, which is recommended, is to fit the two data sets (tracer diffusivities and effective binary diffusivities) separately. The tracer diffusion data of *Watson et al.* [1982] and *Watson* [1991] (excluding the two data points with 11 wt % H_2O_t) may be fit to yield

$$\ln D_{CO_{2,total}} = -8.20 - \frac{22963 + 2.005P}{T} + \left(-1.4262 + \frac{2416.1}{T}\right)C_w. \tag{29}$$

[52] The 2σ uncertainty in predicting ln$D$ is 0.83 for 29 data points (Figure 13b), which is much smaller than the 2σ uncertainty of equation (28), demonstrating the self-consistency of the data of *Watson et al.* [1982] and *Watson* [1991]. The effective binary diffusion coefficients (EBDC) [*Fogel and Rutherford*, 1990; *Zhang and Stolper*, 1991; *Blank et al.*, 1993; *Sierralta et al.*, 2002; *Nowak et al.*, 2004] do not contain enough data at high-H_2O content (only three samples with 0.73, 2.0, and 2.0 wt % H_2O_t). Hence we fit only the 29 data points for "anhydrous" melt ($\leq$0.2 wt % H_2O_t), resulting in

$$\ln D_{CO_{2,total}} = -14.69 - \frac{16915}{T} + 0.2056\frac{P}{T}. \tag{30}$$

[53] The 2σ uncertainty of equation (30) in predicting ln$D$ is 1.06 (Figure 13c), and most of the data by *Nowak et al.* [2004] are somewhat below other data. (In section 3.4 it will be shown that Ar diffusion data of *Nowak et al.* [2004] are also below other data.) The two separate equations (equations (29) and (30)) have better precision than the fit to the combined data set (equation (28)) and hence are

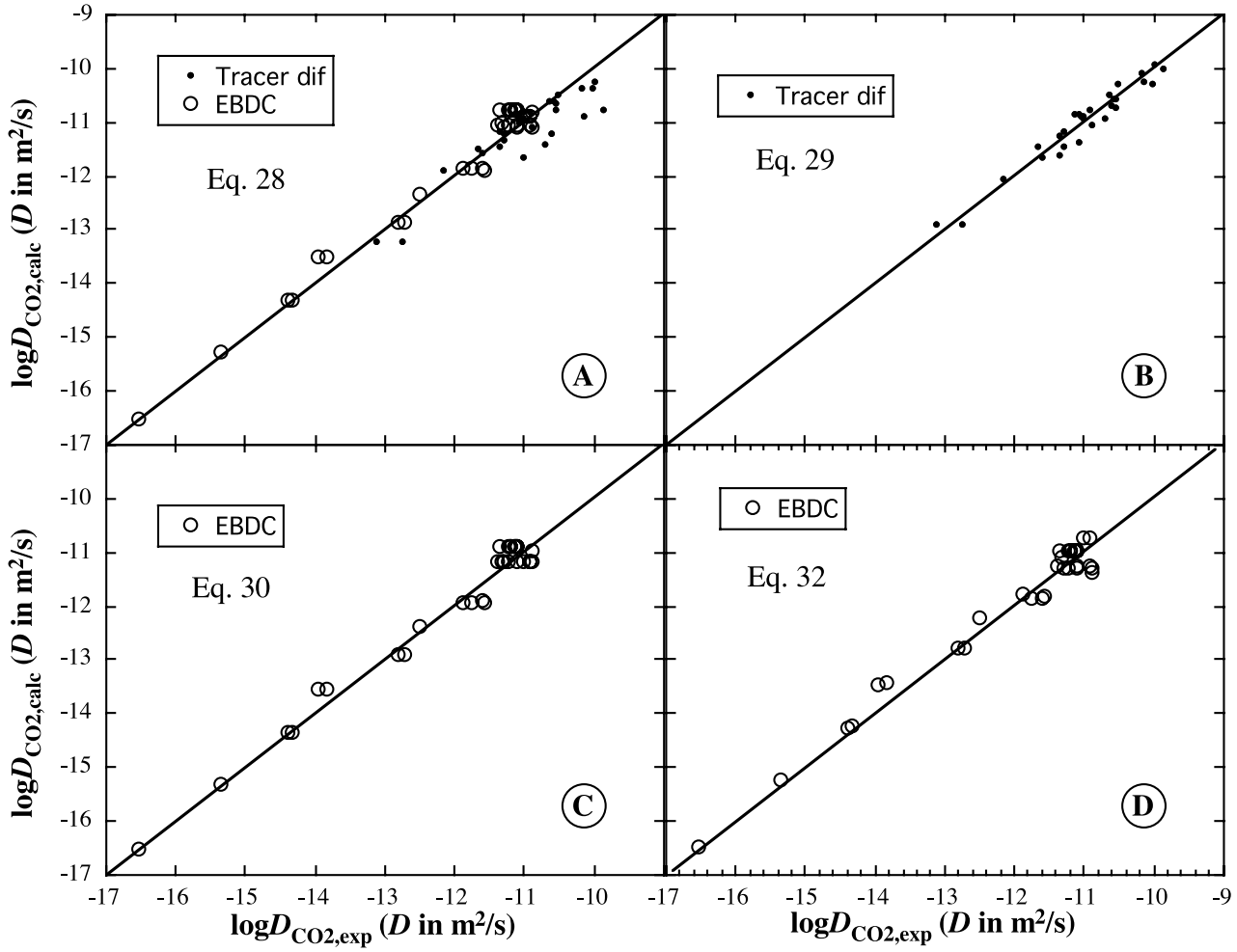

Figure 13. Comparison of experimental data and predictions using different equations: (a) equation (28), (b) equation (29), (c) equation (30), and (d) equation (32). Tracer diffusivity data (solid circles) are from *Watson et al.* [1982] and *Watson* [1991]. Effective binary diffusivity data (open circles) are from *Fogel and Rutherford* [1990], *Zhang and Stolper* [1991], *Blank et al.* [1993], *Sierralta et al.* [2002], and *Nowak et al.* [2004]. Figures 13a, 13b, and 13d include diffusivities in hydrous melts; Figure 13c does not. EBDC is effective binary diffusion coefficients.

temporarily recommended for use under appropriate conditions. Equation (30) cannot be used to estimate EBDC of CO_2 in hydrous rhyolitic to basaltic melts, but it will be shown in section 3.4 that equation (32) derived for Ar diffusivity is applicable to predict CO_2 diffusivity in hydrous melts.

3.3. S Diffusivity in Silicate Melts

[54] Sulfur is the third most abundant volatile component in natural silicate melts. The importance of sulfur as a volcanic gas stems not only from its abundance but more so from the fact that sulfur from volcanic degassing forms aerosols. Hence sulfur emission from major volcanic eruptions often leads to significant cooling of Earth's surface because of its impact on Earth's radiative balance.

[55] Dissolved sulfur in silicate melts may also be present in several species, such as S^{2-}, SO_4^{2-}, SO_2, S_2^{2-}, etc., making it more complicated than H_2O or CO_2. The controlling factor of species concentration ratios for sulfur is oxygen fugacity, different from that for H_2O (H_2O_t content) and CO_2 (anhydrous melt composition). (Under very reducing conditions, H_2O and CO_2 speciation is also controlled by oxygen fugacity.) Unlike the case of H_2O and CO_2, there is no established method to accurately measure the concentrations of different S species.

[56] Sulfur diffusion data in silicate melts are limited [*Watson*, 1994; *Baker and Rutherford*, 1996; *Winther et al.*, 1998; *Freda et al.*, 2005]. In a review paper, *Watson* [1994] "previewed" sulfur diffusion data, but the full data have not been published. *Baker and Rutherford* [1996] obtained sulfur diffusion data in rhyolite melts. *Majewski and Walker* [1998] reported sulfur diffusivity in Fe-Ni-S-P melts, which will not be discussed further because we focus on silicate melts. *Winther et al.* [1998] investigated magmatic sulfur compounds and sulfur diffusion in albitic melt at 1 GPa and 1573–1773 K. *Freda et al.* [2005] studied sulfur diffusion in basaltic melts at 0.1–1 GPa and 1523–1723 K. The data are summarized in auxiliary material Data Set S3.

[57] Curiously, many S diffusion data seem to show large scatter compared to diffusion data of other components. For

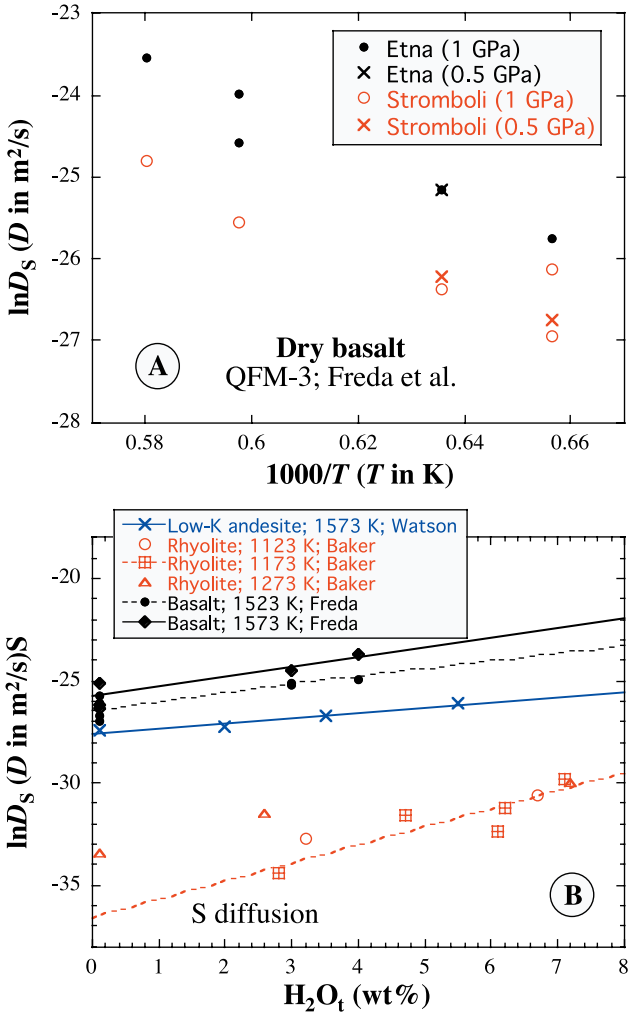

Figure 14. Dependence of sulfur diffusivity on temperature, pressure, and H_2O_t content. Sources of data are *Watson* [1994], *Baker and Rutherford* [1996], and *Freda et al.* [2005].

example, sulfur diffusivity (D_S) from different traverses of a single experiment (experiment 108) varies by a factor of 10 from $10^{-15.92}$ to $10^{-14.92}$ m^2 s^{-1}, and D_S at 1273 K may be smaller than that at 1373 K (experiments 97 and 125) [*Baker and Rutherford*, 1996].

[58] The dependence of S diffusivity on pressure is shown in Figure 14a. The pressure effect is negligible from 0.5 to 1 GPa. Therefore data with different pressures are not distinguished in Figures 14b and 15 for sulfur diffusivity.

[59] The dependence of S diffusivity on H_2O_t is shown in Figure 14b. Sulfur diffusivity increases roughly exponentially with H_2O_t (i.e., ln$D$ is linear to H_2O_t), consistent with the dependence of $D_{H_2O_m}$, $D_{CO_2O_{total}}$, and D_{Ar} on H_2O_t. The rate of D_S increase with H_2O_t appears to depend strongly on composition and/or temperature. For example, D_S increases by 0.14 log units (or 0.32 ln units) per weight percent H_2O_t for andesite at 1573 K [*Watson*, 1994], by 0.21 log units (or 0.48 ln units) per weight percent H_2O_t for basalt at 1573 K [*Freda et al.*, 2005], and by 0.39 log units (or 0.9 ln unit) per weight percent H_2O_t for rhyolitic melt at 1173 K [*Baker and Rutherford*, 1996].

[60] Sulfur diffusivities in some rhyolitic, albitic, dacitic, andesitic, and basaltic melts are shown in Figure 15: (1) For a melt at a given H_2O_t and oxygen buffer, there is a rough Arrhenius relation; (2) S diffusivity increases by about 2.5 orders of magnitude from oxidizing to reducing conditions and by about 2 orders of magnitude from rhyolitic to basaltic composition. For basaltic melts under reducing conditions the dependence of D_S on T and H_2O_t may be estimated. From the data of *Freda et al.* [2005] and ignoring the differences between Etna and Stromboli basalts, D_S in basalt at 1498–1723 K, 0.5–1 GPa, and 0–4 wt % H_2O_t may be described as follows:

$$\ln D_{S\,\text{in basalt}} = -8.21 - \frac{27692 - 651.6C_w}{T}, \qquad (31)$$

where D_S is in m^2 s^{-1}, C_w is H_2O_t content in weight percent, and T is in kelvins.

[61] Because sulfur diffusivity depends on temperature, melt composition (including H_2O_t), and oxygen fugacity, because of the large scatter in data, and because of the limited data available, it is difficult to develop a general equation to predict the diffusivity of sulfur. Some of the complexities and scatter might be due to speciation of sulfur in silicate melts. Therefore it will be important in the future to investigate the speciation of sulfur and the effect of f_{O2} in order to make sense out of the sulfur diffusion data.

3.4. Ar Diffusivity in Silicic Melts

[62] Among minor volatile components, diffusion of Ar has been investigated most extensively [*Reynolds*, 1957; *Perkins and Begeal*, 1971; *Lux*, 1987; *Matsuda et al.*, 1989; *Carroll*, 1991; *Carroll and Stolper*, 1991; *Roselieb et al.*, 1992, 1995, 1996; *Draper and Carroll*, 1995; *Behrens and Zhang*, 2001; *Nowak et al.*, 2004]. In fact, Ar diffusion is

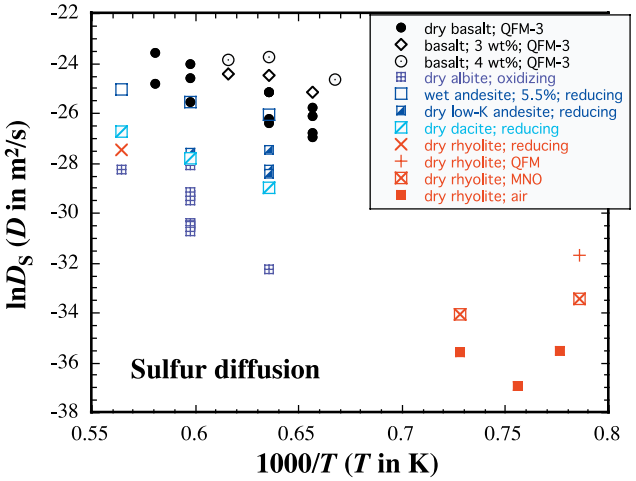

Figure 15. Sulfur diffusion data in rhyolite, albite, dacite, andesite, and basalt melts. Data are from *Watson* [1994], *Baker and Rutherford* [1996], *Winther et al.* [1998], and *Freda et al.* [2005].

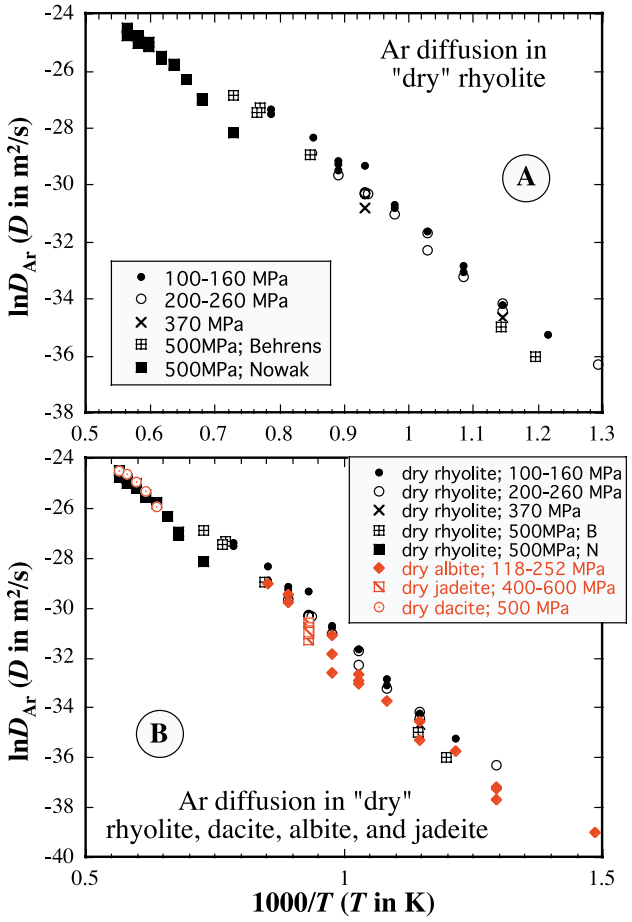

Figure 16. Ar diffusivity versus temperature for (a) rhyolite only and (b) rhyolite, dacite, albite, and jadeite melts. Data are from *Carroll* [1991], *Draper and Carroll* [1995], *Roselieb et al.* [1995], *Behrens and Zhang* [2001], and *Nowak et al.* [2004].

investigated more extensively than diffusion of CO_2 or S and on par with that of H_2O. It has been extensively studied for the following reasons: (1) Ar is a simple monatomic molecule, and understanding its diffusion provides a baseline for understanding the diffusion of more complicated components such as H_2O and CO_2; (2) Ar diffusion in rhyolitic melt has been found to be similar to CO_2 diffusion in the same melt and hence may be used as a proxy for total CO_2 diffusion in all melts (recall that CO_2 diffusivity is almost independent of anhydrous melt composition) and also as a proxy for molecular CO_2 diffusion in rhyolitic melt (recall that in rhyolite CO_2 is present as molecular CO_2); and (3) Ar is relatively easy to analyze by electron microprobe and hence diffusion studies are relatively easy. Compilation of the literature provides about 260 Ar diffusivity data points in various melts (auxiliary material Data Set S4). Ar diffusivity depends on the anhydrous melt composition.

[63] Ar diffusion in dry and wet rhyolitic and haplorhyolitic melts has been investigated by *Matsuda et al.* [1989], *Carroll* [1991], *Draper and Carroll* [1995], *Behrens and Zhang* [2001], and *Nowak et al.* [2004], with 75 data points covering 753–1773 K, 0.1–1500 MPa and 0–5 wt % H_2O_t. The data on anhydrous melts (containing <0.3 wt % H_2O_t) are compared in Figure 16a. Similar to the case of CO_2 diffusion data, Ar diffusivity data by *Nowak et al.* [2004] are slightly off the data by other authors (by about a factor of 2 in D). *Matsuda et al.* [1989] reported Ar diffusivity values at 1073 and 1273 K for a sample containing 2.81 wt % H_2O_t by stepwise heating in a mass spectrometer, but the value at 1273 K was listed to be questionable by the authors. The datum at 1073 K is also significantly off from the trend defined by other literature data (by about a factor of 7). Hence Ar diffusion data of *Matsuda et al.* [1989] are not used.

[64] Figure 16b shows that Ar diffusivities in rhyolitic, dacitic, albitic, and jadeitic melts are similar. We take advantage of the similarity of Ar diffusivities in these melts and fit Ar diffusivities in these melts together. There are 152 data points, including the data of *Nowak et al.* [2004] but excluding the data of *Matsuda et al.* [1989] and one data point at 673 K for albite by *Carroll and Stolper* [1991] because the original authors thought this point was anomalous. These data cover a wide range of temperature, pressure, and H_2O_t content. The fit yields the following equation to predict Ar diffusivity in anhydrous and hydrous rhyolitic, dacitic, albitic, and jadeitic melts:

$$\ln D_{\mathrm{Ar\ in\ silicic\ melts}} = -13.99 - \frac{17367 + 1.9448P}{T} + \frac{(855.2 + 0.2712P)C_w}{T}, \quad (32)$$

where D_{Ar} is Ar diffusivity in $m^2\ s^{-1}$, P is in MPa, T is in kelvins, and C_w is weight percent of H_2O_t. The activation energy and volume for dry melts implied by equation (32) are 144.4 kJ mol^{-1} and 16×10^{-6} m^3 mol^{-1}. The 2σ uncertainty of equation (32) is 0.71 in terms of ln$D$ (or 0.31 in terms of log$D$) (Figure 17). Equation (32) may be applied to rhyolite, dacite, albite, and jadeite melts at 773–1773 K, $P \leq 1$ GPa, and $H_2O_t \leq 5$ wt %.

[65] It has been noted before that total CO_2 diffusivity in all melts is miraculously similar to Ar diffusivity in silicic melts [*Behrens and Zhang*, 2001; *Nowak et al.*, 2004]. This may be explained by the similar size of CO_2 (base radius of 1.40 Å and half-length of 2.5 Å, with a geometric mean of 1.70 Å) and Ar (radius 1.64 Å [*Zhang and Xu*, 1995]) and similar mass (44 versus 40 atomic mass units). The small base radius of CO_2 may compensate its greater half-length so that the linear CO_2 molecule may orient itself and move across the doorways (gaps between adjacent ions of the silicate network) as efficiently as Ar [*Behrens and Zhang*, 2001]. Indeed, equation (32) also predicts the EBDC of CO_2 well (Figures 13d and 17), with a 2σ error of 1.13 in terms of $\ln D_{CO_{2,total}}$, which is similar to that of equation (30) (2σ = 1.06). Hence, although there is not enough data to estimate how EBDC of CO_2 depends on H_2O_t (equation (30) does not include the effect of H_2O_t), we suggest the use of equation (32) to calculate the effective binary diffusivity of CO_2 in anhydrous and hydrous rhyolite to basalt before

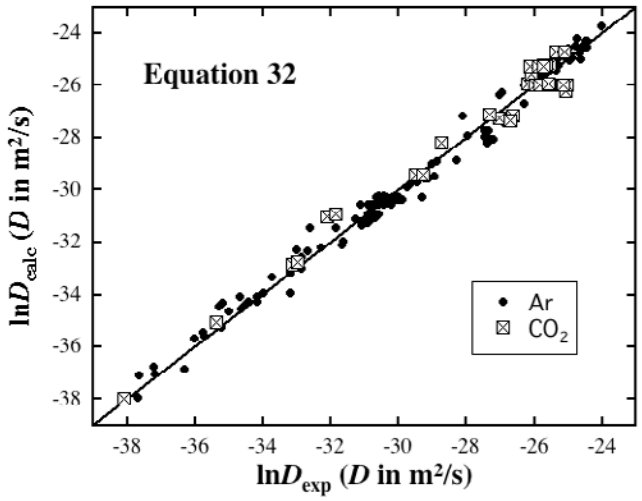

Figure 17. Comparison of experimental data of Ar diffusivity in anhydrous and hydrous silicic melts and chemical diffusion data of $CO_{2,total}$ in all melts with prediction by equation (32). The line is a 1:1 line. For data sources, see captions of Figures 13 and 16.

more CO_2 diffusion data are available. This second application of equation (32) to CO_2 diffusion in all natural silicate melts is probably more important than its primary application to Ar diffusivity in silicic melts.

[66] Ar diffusion in anhydrous silica melt has been investigated by *Perkins and Begeal* [1971], *Carroll and Stolper* [1991], *Draper and Carroll* [1995], and *Roselieb et al.* [1995], with 73 data points covering 673–1178 K and 0.1–372 MPa (Figure 18). Because the diffusivity is well constrained at 0.1 MPa and less well constrained at higher pressures, we first fit the data at 0.1 MPa using the Arrhenius equation and then plot $\Delta \ln D = \ln D_{\text{exp}} - \ln D_{0.1\ \text{MPa,calc}}$ versus pressure to determine the pressure dependence. In essence, we treat the 0.1-MPa data to be more accurate than the higher-pressure data. The expression of D is as follows:

$$\ln D_{\text{Ar in silica melt}} = -18.239 - \frac{14473 + 1.0964P}{T}, \qquad (33)$$

where D is in $m^2\ s^{-1}$, T is in kelvins, and P is in MPa. The 2σ uncertainty of the above expression is 0.70 in terms of $\ln D$ (or 0.3 in terms of $\log D$).

[67] There are limited experimental Ar diffusion data on other melts such as andesite, basalt, orthoclase, and a potassium-lime aluminosilicate [*Reynolds*, 1957; *Lux*, 1987; *Carroll*, 1991; *Nowak et al.*, 2004]. Ar diffusivity increases from rhyolite to basalt by a factor of about 4 at 1573–1773 K and 500 MPa. There are not enough data to derive the dependence of Ar diffusivity on temperature, pressure, and H_2O_t content in these melts. Although the data appear to indicate that the activation energy increases from rhyolite to andesite to basalt, accurate activation energy cannot be obtained for andesite and basalt melt because the temperature range is small. Ar diffusivity in andesitic melt at 1623–1773 K may be roughly estimated by twice the diffusivity given by equation (32), and that in basaltic melt at 1623–1773 K may be roughly estimated as 4 times the diffusivity of equation (32).

[68] Ar diffusivities in rhyolite, dacite, jadeite, and albite melts (polymerized melts) are only slightly higher than those in silica melt and are smaller than those in basaltic melt, seemingly suggesting that the degree of polymerization plays a main role in controlling Ar diffusivity. It is hence somewhat surprising that Ar diffusivity in orthoclase melt (a polymerized melt) is so much (by about a factor of 50) larger than those in other polymerized melts (Figure 18). The much greater diffusivity in orthoclase suggests that Ar diffusivity does not depend monotonically (such as linearly) on either SiO_2 or $SiO_2 + Al_2O_3$ or the degree of polymerization. The large size of holes afforded by orthoclase melt may play a role. Because of this complexity we do not at the moment have a simple way to model the dependence of Ar diffusivity on the melt composition even with such a large data set.

4. GEOSPEEDOMETRY

[69] In this section we briefly discuss the geospeedometer based on the hydrous species reaction (reaction (1)) in rhyolitic melt. This discussion will also be helpful in section 5 on melt viscosity. "Reading" the thermal history of rocks is an important goal of volcanology and petrology. In studying volcanic rocks it is often necessary to estimate the cooling rate in the rock and in different parts of the eruption column, from which the cooling environment and other dynamic information may be inferred [*Tait et al.*,

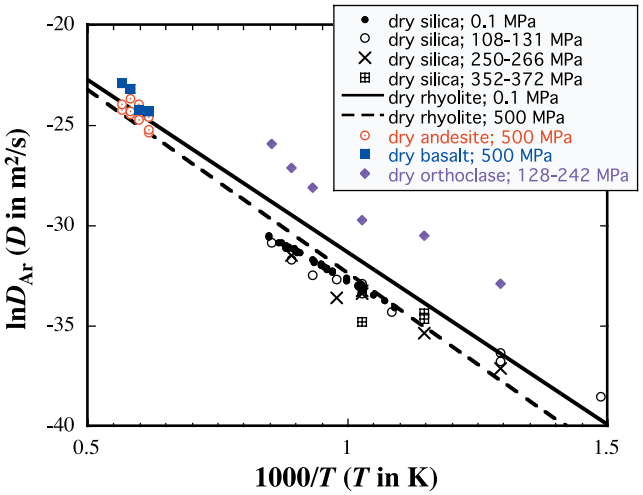

Figure 18. Ar diffusivities in dry silica (black solid circles), andesite (red dotted circles), basalt (blue solid squares), and orthoclase (purple solid diamonds) compared with those in rhyolite (solid and dashed lines calculated from equation (32)) in an Arrhenius plot. Data sources can be found in caption of Figure 16; additional sources are *Reynolds* [1957], *Perkins and Begeal* [1971], *Lux* [1987], and *Carroll and Stolper* [1991].

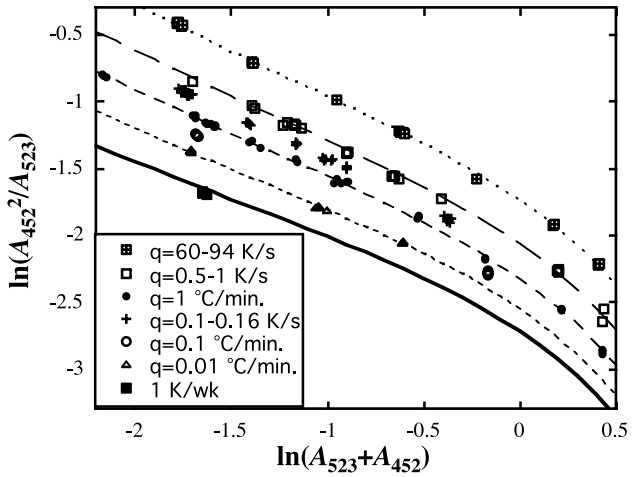

Figure 19. Experimental data relating IR band intensities with cooling rate versus model curves. A_{523} and A_{452} are IR band intensities (peak heights) per millimeter sample thickness at 5230 cm^{-1} and 4520 cm^{-1} using flexicurve baselines [e.g., *Zhang*, 1999a]. Because A_{523} is roughly proportional to H_2O_m content and A_{452} is roughly proportional to OH content, $(A_{523} + A_{452})$ is a proxy for H_2O_t content, and A_{452}^2/A_{523} is a proxy for the equilibrium constant K_2 (equation (2)). The curves (from top down) are calculated using equation (34) for cooling rates of 70 K s^{-1}, 1 K s^{-1}, 1 K min^{-1}, 0.01 K min^{-1}, and 1 K $week^{-1}$. Data are from *Zhang et al.* [1997b, 2000] and *Zhang and Xu* [2007].

1998]. Furthermore, in experimental studies it is also often necessary to know the cooling rate in the experimental apparatus. One geospeedometer (cooling rate indicator) that is especially applicable to volcanic eruptions is based on the kinetics of the hydrous species reaction (reaction (1)) during cooling. The geospeedometer has been calibrated at cooling rate of 10^{-6}–100 K s^{-1} [*Zhang et al.*, 1997b, 2000; *Zhang and Xu*, 2007], a variation of 8 orders of magnitude. The basic principle is as follows [*Zhang*, 1994]: The equilibrium constant of reaction (1) increases with temperature. That is, for a given H_2O_t, equilibrium at higher temperature leads to a higher OH content (i.e., to a higher equilibrium constant K_2) and vice versa. If a hydrous melt is cooled from a high initial temperature (such as 1073 K) rapidly, the melt would spend a short time at each temperature interval and hence less reaction would happen. That is, in the quenched hydrous glass, K_2 would be high, and the apparent equilibrium temperature (T_{ae}) would be high. On the other hand, if the cooling is slow on the same hydrous melt starting from the same initial temperature, K_2 in the cooled glass would be smaller, leading to a lower apparent equilibrium temperature. Hence there is a correlation between the final species concentrations in the cooled glass and the cooling rate, which would serve as a geospeedometer if calibrated.

[70] The kinetics of the reaction was first investigated through isothermal experiments on how species concentrations reach equilibrium [*Zhang et al.*, 1991a, 1995]. It was found that the kinetics is relatively complicated, probably because of the existence of subspecies. Because of this complexity it is difficult to quantify the isothermal kinetics well enough for the development of the geospeedometer. Hence the geospeedometer was calibrated empirically by carrying out controlled cooling rate experiments [*Zhang et al.*, 1997b, 2000; *Zhang and Xu*, 2007]. *Zhang et al.* [1997b] calibrated for a small range of cooling rate and H_2O_t. *Zhang et al.* [2000] extended the calibration. A 2.4-year experiment with very slow cooling rate of 1 K $week^{-1}$ further extended the applicability of the geospeedometer [*Zhang and Xu*, 2007]. These investigations are summarized below.

[71] A hydrous rhyolitic glass with known H_2O_t is heated to an initial temperature at which equilibrium is reached and then cooled down at a given cooling rate (such as 1 K min^{-1}). The initial temperature must be high enough so that there will be significant reaction, and the final species concentrations after cooling down differ significantly from the equilibrium species concentrations at the initial temperature and depend only on the cooling rate but not on the initial temperature. Infrared spectra are taken on the final cooled glass, and the absorbances at 5230 cm^{-1} and 4520 cm^{-1} per unit thickness of the sample (denoted as A_{523} and A_{452}) are obtained. A_{523} is roughly proportional to H_2O_m concentration, and A_{452} is roughly proportional to OH concentration. Furthermore, $(A_{523} + A_{452})$ is roughly proportional to H_2O_t, and $(A_{452})^2/A_{523}$ is roughly proportional to K_2. In order to use the full precision of infrared measurements the absorbances per unit thickness of the sample (A_{523} and A_{452}) are not converted to species concentrations but are directly used in constructing the geospeedometry model (i.e., the cooling rate is related to band intensities). In such treatments, A_{523}, A_{452}, $(A_{523} + A_{452})$, and $(A_{452})^2/A_{523}$ are proxies for H_2O_m, OH, H_2O_t, and K_2. The experimental data are shown in Figure 19. Using experimental data, the following relation between band intensities and cooling rate is obtained

$$z = f(x,y) = -5.4276 - 1.196x - 0.044536y - 0.023054xy + 3.7339e^{0.21361x+0.030617y} - 0.37119e^{1.6299x}, \quad (34)$$

where $x = \ln(A_{523} + A_{452})$, $y = \ln q$, $z = \ln[(A_{452})^2/A_{523}]$, and q is cooling rate in K s^{-1} when the sample temperature equaled T_{ae}. Given A_{523} and A_{452}, x and z can be calculated, and the third parameter y may be solved numerically from equation (34). For ease of calculating q in a spreadsheet program an iteration algorithm is as follows [*Zhang et al.*, 2000]. Define $\xi = \ln[(A_{452})^2/A_{523}]_{x=-1.7}$, which is calculated as follows:

$$\xi = \ln\left[(A_{452})^2/A_{523}\right] + z(-1.7,y) - z(x,y), \quad (35)$$

where A_{523} and A_{452} are measured and $z(-1.7, y)$ and $z(x, y)$ are calculated using equation (34) with a guess of y. Then $y = \ln q$ is calculated from

$$y = \ln q = 8.7905 + 7.8096\xi - 3.4937\xi^2. \quad (36)$$

[72] In the iteration the y value thus obtained is applied to equation (35) to calculate ξ, which is then used to calculate a new y value and so on. Iteration using equations (35) and (36) reproduces experimental data of *Zhang et al.* [2000] with the same precision as equation (34). New data by *Zhang and Xu* [2007] show that the iteration algorithm using equations (35) and (36) is more accurate for extrapolating to lower cooling rates (down to 10^{-6} K s^{-1}) than simply using equation (34). Hence the algorithm using equations (35) and (36) is recommended. The 2σ uncertainty in predicting ln$q$ is about 0.5 (or 0.22 in terms of log$q$) for cooling rate range of 10^{-6}–100 K s^{-1} when IR measurement precision of A_{523} and A_{452} is 1% relative or better.

[73] An example of calculation is as follows. Suppose A_{523} and A_{452} from IR measurements on a natural hydrous rhyolitic glass are 0.0748 mm^{-1} and 0.1178 mm^{-1}. Find $x = \ln(A_{523} + A_{452}) = -1.647$ and $z = \ln[(A_{452})^2/A_{523}] = -1.685$. Solving for ln$q$ from equations (35) and (36), we obtain $y = \ln q = -13.7$, leading to $q = 7.7 \times 10^{-7}$ K s^{-1} = 0.097 K d^{-1}.

[74] The geospeedometer has been applied to estimate cooling rate in experimental apparatus [*Zhang et al.*, 2000], of obsidian pyroclasts [*Zhang et al.*, 2000, *Xu and Zhang*, 2002; *Wallace et al.*, 2003], and in eruption columns [*Xu and Zhang*, 2002]. The same data of controlled cooling rate experiments may also be applied to infer viscosity (see section 5).

5. VISCOSITY OF NATURAL SILICATE MELTS

[75] Viscosity of silicate melts is a basic property of melts and is critical in modeling volcanic eruptions. Over the last 40 years many investigators have carried out experiments on natural or nearly natural silicate melts [e.g., *Friedman et al.*, 1963; *Shaw*, 1963; *Kushiro et al.*, 1976; *Persikov et al.*, 1986; *Persikov*, 1991; *Neuville et al.*, 1993; *Stein and Spera*, 1993; *Hess et al.*, 1995, 2001; *Hess and Dingwell*, 1996; *Dingwell et al.*, 1996, 1998a, 1998b, 2000, 2004; *Dorfman et al.*, 1996; *Richet et al.*, 1996; *Scaillet et al.*, 1996; *Schulze et al.*, 1996; *Toplis et al.*, 1997; *Stevenson et al.*, 1998; *Holtz et al.*, 1999; *Giordano et al.*, 2000, 2004a; *Whittington et al.*, 2000, 2001, 2005; *Gottsmann et al.*, 2002; *Giordano and Dingwell*, 2003a; *Liebske et al.*, 2003; *Romano et al.*, 2003; *Zhang et al.*, 2003; *Goto et al.*, 2005; *Zhang and Xu*, 2007]. Many other papers reported viscosity data on melts different from natural melts, which are not included in this review.

[76] Most workers used physical measurements to determine viscosity, including concentric cylinder viscometry and the falling sphere method for relatively low viscosities ($<10^5$ Pa s) and the parallel plate and micropenetration methods for high viscosities (10^9–10^{15} Pa s). *Zhang et al.* [2003] and *Zhang and Xu* [2007] inferred viscosity (10^9–10^{17} Pa s) using controlled cooling rate kinetic experiments on the hydrous species reaction (reaction (1)). Because the method is not conventional, it is explained below. In this method the same data for calibration of the hydrous species geospeedometer (see section 4) are employed to infer viscosity through the following equation [*Zhang et al.*, 2003]:

$$\eta|_{\text{at } T\text{ae}} = \eta|_{\text{at } T\text{g}} = \frac{10^{11.45}}{q}, \tag{37}$$

where η is viscosity in Pa s, q is cooling rate in K s^{-1}, the units of the constant $10^{11.45}$ are Pa K, and T_{ae} is the apparent equilibrium temperature in a cooled melt (glass) after a controlled cooling rate experiment. For a controlled cooling rate experiment, q is known. Hence, in this method the temperature (T_{ae}) is measured from IR band intensities after the experiment to obtain a η-T-H_2O_t data point.

[77] Experimental viscosity data have been employed to calibrate viscosity models as a function of temperature and melt composition including H_2O content [e.g., *Bottinga and Weill*, 1972; *Shaw*, 1972; *Persikov*, 1991; *Hess and Dingwell*, 1996; *Spera*, 2000; *Giordano and Dingwell*, 2003b; *Zhang et al.*, 2003; *Giordano et al.*, 2004b; *Russell and Giordano*, 2005; *Hui and Zhang*, 2007]. *Bottinga and Weill* [1972] and *Shaw* [1972] were pioneers in developing general viscosity models for natural silicate melts. *Persikov* [1991] developed a new viscosity model for melts at high temperatures (i.e., for viscosity $<10^5$ Pa s), improving on that of *Shaw* [1972]. The viscosity models of *Bottinga and Weill* [1972] and *Shaw* [1972] had been widely used for over 20 years because it was extremely difficult to develop better models [*Lange*, 1994]. In these early models the dependence of viscosity on temperature is assumed to be Arrhenian ($\log\eta = A_0 + A_1/T$), which works well over a small viscosity range (such as 0.1–10^4 Pa s). Later data at high viscosities (10^9–10^{15} Pa s) showed that a simple Arrhenian relation does not work over a large viscosity range. Recently, more advanced models and relationships accounting for the non-Arrhenian behavior have been developed. *Hess and Dingwell* [1996] developed the first non-Arrhenian viscosity model incorporating the dependence of viscosity on H_2O_t content. The model was based on the Vogel-Fulcher-Tammann (VFT) equation $\log\eta = A_0 + A_1/(T - A_2)$ and was widely applied. Because the model has a relatively large 2σ uncertainty (0.92 units in logη) and cannot apply to completely dry rhyolitic melt, *Zhang et al.* [2003] formulated a different non-Arrhenian viscosity model using $\log\eta = A_0 + (A_1/T)^n$ (where n is a parameter to be determined from experimental data) that is applicable to both dry and hydrous rhyolitic melt and has a smaller 2σ uncertainty (0.36 units in logη). *Giordano et al.* [2004b] advanced another non-Arrhenian viscosity model based on the VFT equation, which applies to both dry and hydrous silicic melt with 2σ uncertainty of about 0.4 units in logη. They also generated a viscosity model for silicic melts containing both H_2O and F with 2σ uncertainty of about 0.6 units in logη. For more general melt compositions, two non-Arrhenian models have been advanced [*Giordano and Dingwell*, 2003b; *Hui and Zhang*, 2007]. The viscosity model of *Giordano and Dingwell* [2003b] is for all anhydrous melts at temperature >700°C, and the 2σ uncertainty is 0.78 log units. The viscosity model of *Hui and Zhang*

[2007] covers all natural and nearly natural (such as iron free) dry and hydrous silicate melt compositions and all experimental temperatures, with a 2σ uncertainty of 0.61 in terms of $\log\eta$.

[78] The general viscosity model of *Hui and Zhang* [2007] for natural silicate melts is based on the empirical relation of $\log\eta = A_0 + A_1/T + \exp(A_2 + A_3/T)$, where A_0, A_1, A_2, and A_3 are parameters depending roughly linearly on composition. The full expression as follows is somewhat complicated:

$$\begin{aligned}\log\eta = {} & \big[-6.83X_{SiO_2} - 170.79X_{TiO_2} - 14.71X_{Al2O3,ex} \\ & - 18.01X_{MgO} - 19.76X_{CaO} + 34.31X_{(Na,K)2Oex} \\ & - 140.38Z + 159.26X_{H_2O} - 8.43X_{(Na,K)_{AlO_2}}\big] \\ & + 1000\big[18.14X_{SiO_2} + 248.93X_{TiO_2} \\ & + 32.61X_{Al2O3,ex} + 25.96X_{MgO} + 22.64X_{CaO} \\ & - 68.29X_{(Na,K)2Oex} + 38.84Z - 48.55X_{H_2O} \\ & + 16.12X_{(Na,K)_{AlO_2}}\big]/T + \exp\big\{\big[21.73X_{Al2O3,ex} \\ & - 61.98X_{(Fe,Mn)O} - 105.53X_{MgO} \\ & - 69.92X_{CaO} - 85.67X_{(Na,K)2Oex} + 332.01Z \\ & - 432.22X_{H_2O} - 3.16X_{(Na,K)_{AlO_2}}\big] \\ & + 1000\big[2.16X_{SiO_2} - 143.05X_{TiO_2} - 22.1X_{Al2O3,ex} \\ & + 38.56X_{(Fe,Mn)O} + 110.83X_{MgO} \\ & + 67.12X_{CaO} + 58.01X_{(Na,K)2Oex} + 384.77X_{P_2O_5} \\ & - 404.97Z + 513.75X_{H_2O}\big]/T\big\}, \end{aligned} \tag{38}$$

where η is viscosity in Pa s, X_i are oxide mole fractions (X_{H_2O} means mole fraction of H_2O_t), $Z = (X_{H_2O})^{1/[1+(185.797/T)]}$, and $Al_2O_{3,ex}$ or $(Na, K)_2O_{ex}$ means excess oxides after forming $(Na,K)AlO_2$. The model covers anhydrous and hydrous, rhyolitic to peridotitic, and peralkaline to peraluminous melts at both high and low temperatures. The conditions covered by the model are $H_2O_t \le 5$ wt % (except for rhyolitic melt for which $H_2O_t \le 12.3$ wt %), $P \le 500$ MPa, 573 K $\le T \le$ 1978 K, and 0.1 Pa s $\le \eta \le 10^{15}$ Pa s. The 2σ deviation of the fit is 0.61 $\log\eta$ units. Although the model contains many parameters, it is easy to include in software codes or spreadsheet programs. We recommend its use in modeling volcanic and magmatic processes, but (1) no extrapolation should be attempted because of the complicated form of the equation, and (2) for specific melts, there may be more accurate viscosity models.

[79] In addition to the calculation of viscosity, equations (37) and (38) may also be applied to calculate the glass transition temperature for any given melt composition and cooling rate. For example, for a hydrous basaltic melt (50 wt % SiO_2, 1.5 wt % TiO_2, 15% Al_2O_3, 10% FeO, 0.2% MnO, 9% MgO, 10% CaO, 3% Na_2O, 0.4% K_2O, 0.2% P_2O_5, and 0.7% H_2O_t) at a cooling rate of 100 K s^{-1} the glass transition would occur at viscosity = $10^{11.45}/100 = 10^{9.45}$ Pa s (equation (37)). Then using equation (38), the glass transition temperature (i.e., the temperature at which the viscosity is $10^{9.45}$ Pa s) is 932 K.

[80] Because the viscosity model (equation (38)) is general for all melt compositions, it may also be used to estimate cooling rate of hydrous glass of other natural melt compositions (equation (34) is for hydrous rhyolitic melt only), although the uncertainty is relatively large (about a factor of 4). For example, if the above hydrous basaltic glass with 0.7 wt % H_2O_t has a T_{ae} of 850 K, the viscosity at this temperature is $10^{12.0}$ Pa s, meaning that the cooling rate at 850 K is $10^{11.45}/10^{12.0} \approx 0.3$ K s^{-1}. However, if T_{ae} for a hydrous basaltic glass is 780 K, the calculated viscosity would be $10^{16.3}$ Pa s, exceeding the limit of the calibration, which means that the viscosity and hence cooling rate cannot be reliably inferred.

[81] The above discussion is for relaxed viscosity (or Newtonian viscosity) only, meaning viscosity at small strain rate. If the strain rate is high, viscosity decreases with the strain rate (referred to as shear thinning behavior). The strain rate–dependent (SRD) viscosity may be expressed as follows [*Webb and Dingwell*, 1990; *Simmons*, 1998; *Gonnermann and Manga*, 2007]:

$$\eta^* = \frac{\eta}{1 + \kappa\dot{\varepsilon}}, \tag{39}$$

where η is the relaxed shear viscosity (equation (38)), η^* is the strain rate–dependent shear viscosity, $\dot{\varepsilon}$ is strain rate in s^{-1}, and κ is a coefficient depending on η. Approximately, $\kappa \approx 3.5 \times 10^{-6}\eta^{0.76}$, where η is in Pa s and κ is in seconds. For example, if $\dot{\varepsilon} = 0.1$ s^{-1} (extremely high strain rate), $\eta = 10^{10}$ Pa s, then the SRD viscosity $\eta^* = 10^{8.83}$ Pa s, significantly smaller than the relaxed viscosity η.

6. MAGMA FRAGMENTATION

[82] The fragmentation of magma is a necessary though not sufficient condition [*Gonnermann and Manga*, 2003] for explosive volcanic eruption. Before fragmentation, volcanic eruption is a bubbly magma flow (liquid flow). With fragmentation, bubble walls break and gas is released, leading to a volcanic gas containing magma particles. If the fragmentation is extensive, the eruption becomes an explosive eruption, i.e., a violent volcanic gas flow carrying magma particles (Figure 1). Seemingly benign lava flows or domes may suddenly fragment into a killing pyroclastic flow [*Sato et al.*, 1992]. It is hence critical to understand the criteria for magma fragmentation. The discussion below focuses mostly on silicic melts.

[83] Several fragmentation criteria have been proposed. An earlier simple and widely known proposal was that fragmentation would occur if vesicularity exceeds some critical value such as 74%. It was shown later that fragmentation occurs over a wide range of vesicularity [*Cashman and Mangan*, 1994; *Thomas et al.*, 1994; *Zhang et al.*, 1997c; *Spieler et al.*, 2004]. More sophisticated models consider the brittle failure of the bubbly magma [*McBirney and Murase*, 1970; *Alidibirov*, 1994; *Papale*, 1999b; *Zhang*, 1999b]. *McBirney and Murase* [1970] treated the bulk elastic property and strength of the bubbly magma and suggested that fragmentation occurs when the bulk stress on the magma exceeds the bulk strength of the bubbly magma.

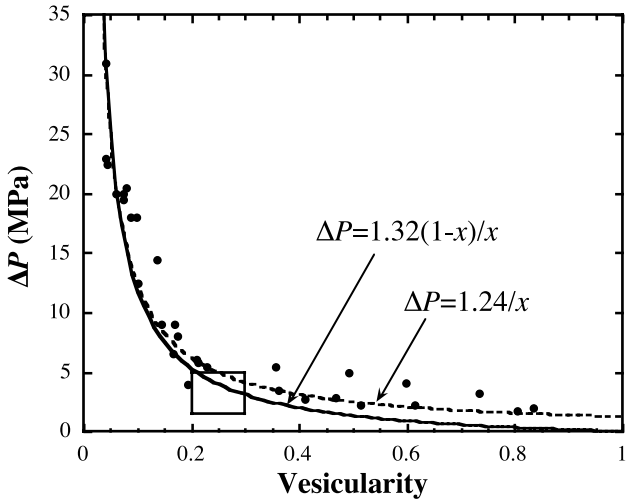

Figure 20. Experimental data on the required pressure differential ΔP_c for magma fragmentation (dots [*Spieler et al.*, 2004]) and for decrepitation of H_2O bubbles in glasses containing 5–6 wt % H_2O (rectangle [*Romano et al.*, 1996]). The solid curve is a fit to the data by $\Delta P_c = S(1 - \phi)/\phi$, where ϕ is vesicularity and S is tensile strength. The dashed curve is a fit by the equation $\Delta P = Y/\phi$, where ϕ is vesicularity and Y is a fitting parameter related to strength.

Alidibirov [1994] addressed the stress distribution surrounding a thin-walled bubble and suggested a couple of fragmentation criteria. *Papale* [1999b] proposed that fragmentation of magma would occur if the magma strain rate exceeds the relaxation rate. *Zhang* [1999b] evaluated the maximum tensile stress in the bubble wall and suggested that fragmentation would occur when the tensile stress on the inner wall of bubbles exceeds the strength of the melt. Quantitative theories were developed in each of these four works.

[84] A major advance was made recently in the understanding of magma fragmentation. *Spieler et al.* [2004] carried out a series of shock-tube experiments to investigate the condition for fragmentation. The apparatus (the fragmentation bomb) consists of a pressure vessel and a large 1-atm steel tank separated by a system of three scored diaphragms that open at a prescribed pressure differential. The starting samples were solid. A piece of natural pumice is characterized for its open (or interconnected) and total vesicularity by examining thin sections. It turns out that 75–99.5% of the total vesicularity in the pumice samples used in the experiments is open vesicularity. A cylinder is prepared from the pumice and placed into the fragmentation bomb. The sample is then heated to 850°C and compressed with Ar until the diaphragm opens. If the pressure differential is not high enough, the pumice cylinder does not fragment. If the pressure differential is high enough, there is fragmentation. The pressure differential required for fragmentation is recorded as a function of vesicularity. The data are shown in Figure 20. Samples from different volcanoes (Unzen, Etna, Merapi, Santorini, and Montserrat) show roughly consistent trends.

[85] *Spieler et al.* [2004] show that their experimental data are well fit by the simple equation

$$\Delta P_c = \frac{Y}{\phi}, \tag{40}$$

where ΔP_c is the critical pressure difference between the bubble and ambient pressures for fragmentation to occur, ϕ is vesicularity, and Y is a fitting parameter (found to be 1 MPa) related to the tensile strength of the melt. The theory of *Zhang* [1999b] was found to be especially in error at small vesicularities. *Spieler et al.* [2004] pointed out that brittle failure at the inner wall in the model of *Zhang* [1999b] only indicates initiation of cracking but not necessarily complete breakup of the bubble. It can be shown [*Koyaguchi and Mitani*, 2005; T. Koyaguchi, personal communication, 2004] that if the theory of *Zhang* [1999b] is modified to consider the tensile stress on the outer wall of melt shell of the bubble using the results of *Zhang* [1998b], the critical pressure difference would be

$$\Delta P_c = \frac{S(1-\phi)}{\phi}, \tag{41}$$

where S is the tensile strength of the material. Equation (41) fits the experimental data well. This equation would also satisfy the limiting condition that the critical pressure is zero if vesicularity is 1 (meaning infinitely thin bubble walls). Because of the similarity between equations (40) and (41), the physical meaning of the empirical equation (40) can be seen to reflect that fragmentation occurs when the stress on the melt shell exceeds the strength of the melt.

[86] The following differences might affect the applicability of the theoretical and experimental approach to fragmentation in nature: (1) In theoretical treatments mentioned above, closed pores are assumed; (2) in the experimental study of *Spieler et al.* [2004] most pores are open pores, whereas (3) in natural magma before fragmentation the proportion of open pores to closed pores is not known. For example, one might argue that prior to magma fragmentation in nature most pores are closed pores, but many become open pores during fragmentation and during pumice solidification. More recent studies suggest that increasing permeability (related to the degree of connectedness of the vesicles) may shift fragmentation threshold to higher ΔP than predicted by equation (40) [*Mueller et al.*, 2005; *Gonnermann and Manga*, 2007]. Despite some uncertainties the work by *Spieler et al.* [2004] represents a major advance in understanding magma fragmentation.

[87] Several other studies investigated a spectrum of processes following rapid decompression of analog gas-bearing liquids or viscoelastic materials [e.g., *Mader et al.*, 1994, 1996, 1997; *Zhang et al.*, 1997c; *Zhang*, 1998a; *Ichihara et al.*, 2002; *Namiki and Manga*, 2005]: bubble nucleation, bubble growth and expansion, eruption velocity, detachment, partial rupture, and fragmentation. Two of these studies in particular addressed the issue of fragmentation. *Ichihara et al.* [2002] noted that for a bubble-bearing

viscoelastic material (dilatant silicone compound), fragmentation depends on both ΔP and the decompression rate. *Namiki and Manga* [2005] determined that for another bubble-bearing viscoelastic fluid (xanthan gum solution), fragmentation also depends on initial vesicularity (ϕ) and overpressure (ΔP), but the relation is somewhat different from equation (40) and is quantified using potential energy.

7. SUMMARY

[88] After years of effort by numerous scientists the understanding of some melt properties begins to allow realistic modeling of volcanic eruption dynamics and magmatic processes. Below is a brief summary of the current understanding of the following melt properties:

[89] 1. H_2O and CO_2 solubility in rhyolitic melt is well understood, and the solubility in pure H_2O or CO_2 vapor and in H_2O-CO_2 mixed vapor may be estimated using equations (7) and (8) at 973–1473 K and 0–500 MPa. The two equations may also be roughly applied to estimate H_2O and CO_2 solubility in other melts. A slightly more accurate equation for predicting H_2O solubility in various melts (rhyolite to basalt) in equilibrium with a pure H_2O vapor is equation (10) at 971–1623 K and 0–800 MPa. For more general conditions and intermediate pressures, equation (9) and the programs of *Newman and Lowenstern* [2002] and *Papale et al.* [2006] may be used.

[90] 2. Total H_2O diffusivity ($D_{H_2O_t}$) depends on temperature, its own concentration, and the anhydrous melt composition. The pressure dependence is only resolved for rhyolite. At relatively low H_2O content, $D_{H_2O_t}$ is roughly proportional to H_2O_t and may be estimated using equation (15) for rhyolite (773–1473 K, $P \leq 0.8$ GPa, and $H_2O_t \leq 2$ wt %), equation (17) for dacite (773–1573 K, $P \leq 1.5$ GPa, and $H_2O_t \leq 0.8$ wt % at about 800 K and $H_2O_t \leq 6$ wt % at about 1500 K), equation (20) for trachyte (1323–1573 K, $P = 1$ GPa, and $H_2O_t \leq 2$ wt %), equation (19) for andesite (773–1573 K, $P \leq 1.5$ GPa, and $H_2O_t \leq 1$ wt % at about 800 K and $H_2O_t \leq 6$ wt % at about 1500 K), and equation (18) for basalt (773–1573 K, $P \leq 1$ GPa, and $H_2O_t \leq 1$ wt %). At higher H_2O contents, only for rhyolite may $D_{H_2O_t}$ be estimated using equation (16) (at 773–1473 K, $P \leq 0.8$ GPa, and $H_2O_t \leq 8$ wt %).

[91] 3. CO_2 diffusivity does not depend on its own concentration and is roughly independent of the anhydrous melt composition. Effective binary or chemical diffusivity of CO_2 in all melts is roughly the same as Ar chemical diffusivity in silicic melts. Both may be estimated using equation (32) at 773–1773 K, $P \leq 1$ GPa, and $H_2O_t \leq 5$ wt %.

[92] 4. Cooling rate of quenched hydrous rhyolitic glasses may be estimated using equations (35) and (36) at $P \leq 0.5$ GPa, $H_2O_t \leq 8$ wt %, and cooling rate between 10^{-6} and 100 K s^{-1}.

[93] 5. Viscosity of all natural silicate melts may be estimated using equation (38) at 573–1978 K, $P \leq 0.5$ GPa, $H_2O_t \leq 5$ wt % (for rhyolite, H_2O_t may be as high as 12 wt %), and viscosity between 0.1 and 10^{15} Pa s.

[94] This review only covers silicate melt properties. Properties of magmas containing crystals and bubbles are more complicated and require additional considerations. For example, if one needs to estimate the total mass of dissolved volatiles in magma and if all phenocrysts are anhydrous, it is necessary to multiply the total magma mass by the mass fraction of the melt and then by the solubility. For both diffusivity in a magma and viscosity of magma the liquid region of the magma may be treated using equations in this review on a scale much smaller than the mean distance between phenocrysts. On a scale much larger than the mean distance between phenocrysts, the tortuosity of the diffusion path [*Berner*, 1980] and the effect of suspension particles on viscosity [*Petford*, 2003; *Llewellin and Manga*, 2005] must be considered.

[95] **ACKNOWLEDGMENTS.** Part of this paper is related to a course run by Y. Zhang at Peking University. In addition to the students who are coauthors of this paper (M. Zhu and H. Wang), others who participated in the course and/or work include Zhixue Du, Junjie Liu, Long Hu, Qiang Sun, Suhua Cheng, Jin Li, Min Li, Jinping Qi, Erwei Qiao, Huai Wang, Qianjie Wang, Rui Wang, Shixiang Wang, Yinjia Wang, Yu Wang, Yuping Yang, Rui Zhang, Wentao Zhang, and Xingzhi Zhou. We thank Eric Essene, M. Manga, D. Sahagian, E. B. Watson, and an anonymous reviewer for insightful and constructive comments, T. Koyaguchi for discussion on fragmentation, and P. Papale for calculation results using his solubility model. This work is partially supported by Peking University (985 Program by the Chinese Ministry of Education), the Chinese NSFC (40325005), and the US NSF (EAR-0537598).

[96] The Editor responsible for this paper was Michael Manga. He thanks technical reviewers Dork Sahagian and Bruce Watson and one anonymous cross-disciplinary reviewer.

REFERENCES

Alidibirov, M. A. (1994), A model for viscous magma fragmentation during volcanic blasts, *Bull. Volcanol.*, *56*, 459–465.

Baker, L. L., and M. J. Rutherford (1996), Sulfur diffusion in rhyolite melts, *Contrib. Mineral. Petrol.*, *123*, 335–344.

Behrens, H., and N. Jantos (2001), The effect of anhydrous composition on water solubility in granitic melts, *Am. Mineral.*, *86*, 14–20.

Behrens, H., and Y. Zhang (2001), Ar diffusion in hydrous silicic melts: Implications for volatile diffusion mechanisms and fractionation, *Earth Planet. Sci. Lett.*, *192*, 363–376.

Behrens, H., Y. Zhang, and Z. Xu (2004), H_2O diffusion in dacitic and andesitic melts, *Geochim. Cosmochim. Acta*, *68*, 5139–5150.

Behrens, H., Y. Zhang, M. Leschik, M. Miedenbeck, G. Heide, and G. H. Frischat (2007), Molecular H_2O as carrier for oxygen diffusion in hydrous silicate melts, *Earth Planet. Sci. Lett.*, *254*, 69–76.

Berner, R. A. (1980), *Early Diagenesis: A Theoretical Approach*, Princeton Univ. Press, Princeton, N. J.

Blank, J. G. (1993), An experimental investigation of the behavior of carbon dioxide in rhyolitic melt, Ph.D. thesis, 210 pp., Calif. Inst. of Technol., Pasadena.

Blank, J. G., E. M. Stolper, and M. R. Carroll (1993), Solubilities of carbon dioxide and water in rhyolitic melt at 850°C and 750 bars, *Earth Planet. Sci. Lett.*, *119*, 27–36.

Bottinga, Y., and D. F. Weill (1972), The viscosity of magmatic silicate liquids: A model for calculation, *Am. J. Sci.*, *272*, 438–475.

Burn, I., and J. P. Roberts (1970), Influence of hydroxyl content on the diffusion of water in silica glass, *Phys. Chem. Glasses*, *11*, 106–114.

Burnham, C. W. (1975), Water and magmas: A mixing model, *Geochim. Cosmochim. Acta*, *39*, 1077–1084.

Burnham, C. W., and R. H. Jahns (1962), A method for determining the solubility of water in silicate melts, *Am. J. Sci.*, *260*, 721–745.

Carroll, M. R. (1991), Diffusion of Ar in rhyolite, orthoclase and albite composition glasses, *Earth Planet. Sci. Lett.*, *103*, 156–168.

Carroll, M. R., and E. M. Stolper (1991), Argon solubility and diffusion in silica glass: Implications for the solution behavior of molecular gases, *Geochim. Cosmochim. Acta*, *55*, 211–225.

Cashman, K. V., and M. T. Mangan (1994), Physical aspects of magmatic degassing II. Constraints on vesiculation process from textural studies of eruptive products, in *Volatiles in Magmas*, vol. 30, edited by M. R. Carroll and J. R. Holloway, pp. 447–478, Mineral. Soc. of Am., Washington, D. C.

Cockram, D. R., Z. Haider, and G. J. Roberts (1969), The diffusion of "water" in soda-lime glass within and near the transformation range, *Phys. Chem. Glasses*, *10*, 18–22.

Delaney, J. R., and J. L. Karsten (1981), Ion microprobe studies of water in silicate melts: Concentration-dependent water diffusion in obsidian, *Earth Planet. Sci. Lett.*, *52*, 191–202.

Dingwell, D. B., C. Romano, and K. Hess (1996), The effect of water on the viscosity of a haplogranitic melt under P-T-X conditions relevant to silicic volcanism, *Contrib. Mineral. Petrol.*, *124*, 19–28.

Dingwell, D. B., F. Holtz, and H. Behrens (1997), The solubility of H_2O in peralkaline and peraluminous granitic melts, *Am. Mineral.*, *82*, 434–437.

Dingwell, D. B., K. U. Hess, and C. Romano (1998a), Extremely fluid behavior of hydrous peralkaline rhyolites, *Earth Planet. Sci. Lett.*, *158*, 31–38.

Dingwell, D. B., K. U. Hess, and C. Romano (1998b), Viscosity data for hydrous peraluminous granitic melts: Comparison with a metaluminous model, *Am. Mineral.*, *83*, 236–239.

Dingwell, D. B., K. H. Hess, and C. Romano (2000), Viscosities of granitic (sensu lato) melts: Influence of the anorthite component, *Am. Mineral.*, *85*, 1342–1348.

Dingwell, D. B., P. Courtial, D. Giordano, and A. R. L. Nichols (2004), Viscosity of peridotite liquid, *Earth Planet. Sci. Lett.*, *226*, 127–138.

Dixon, J. E., E. M. Stolper, and J. R. Delaney (1988), Infrared spectroscopic measurements of CO_2 and H_2O in Juan de Fuca Ridge basaltic glasses, *Earth Planet. Sci. Lett.*, *90*, 87–104.

Dixon, J. E., E. M. Stolper, and J. R. Holloway (1995), An experimental study of water and carbon dioxide solubilities in mid-ocean ridge basaltic liquids. part I: Calibration and solubility models, *J. Petrol.*, *36*, 1607–1631.

Doremus, R. H. (1969), The diffusion of water in fused silica, in *Reactivity of Solids*, edited by J. W. Mitchell et al., pp. 667–673, John Wiley, New York.

Doremus, R. H. (2004), Transport of oxygen in silicate glasses, *J. Non Cryst. Solids*, *349*, 242–247.

Dorfman, A., K. Hess, and D. B. Dingwell (1996), Centrifuge-assisted falling sphere viscometry, *Eur. J. Mineral.*, *8*, 507–514.

Draper, D. S., and M. R. Carroll (1995), Argon diffusion and solubility in silicic glasses exposed to an Ar-He gas mixture, *Earth Planet. Sci. Lett.*, *132*, 15–24.

Drury, T., and J. P. Roberts (1963), Diffusion in silica glass following reaction with tritiated water vapor, *Phys. Chem. Glasses*, *4*, 79–90.

Fogel, R. A., and M. J. Rutherford (1990), The solubility of carbon dioxide in rhyolitic melts: A quantitative FTIR study, *Am. Mineral.*, *75*, 1311–1326.

Freda, C., D. R. Baker, C. Romano, and P. Scarlato (2003), Water diffusion in natural potassic melts, *Geol. Soc. Spec. Publ.*, *213*, 53–62.

Freda, C., D. R. Baker, and P. Scarlato (2005), Sulfur diffusion in basaltic melts, *Geochim. Cosmochim. Acta*, *69*, 5061–5069.

Friedman, I., W. Long, and R. L. Smith (1963), Viscosity and water content of rhyolitic glass, *J. Geophys. Res.*, *68*, 6523–6535.

Gardner, J. E., M. Hilton, and M. R. Carroll (1999), Experimental constraints on degassing of magma: Isothermal bubble growth during continuous decompression from high pressure, *Earth Planet. Sci. Lett.*, *168*, 201–218.

Giordano, D., and D. Dingwell (2003a), Viscosity of hydrous Etna basalt: Implications for Plinian-style basaltic eruptions, *Bull. Volcanol.*, *65*, 8–14.

Giordano, D., and D. B. Dingwell (2003b), Non-Arrhenian multicomponent melt viscosity: A model, *Earth Planet. Sci. Lett.*, *208*, 337–349.

Giordano, D., D. Dingwell, and C. Romano (2000), Viscosity of a Teide phonolite in the welding interval, *J. Volcanol. Geotherm. Res.*, *103*, 239–245.

Giordano, D., C. Romano, P. Papale, and D. Dingwell (2004a), The viscosity of trachyte, and comparison with basalts, phonolites, and rhyolites, *Chem. Geol.*, *213*, 49–61.

Giordano, D., C. Romano, D. Dingwell, B. Poe, and H. Behrens (2004b), The combined effects of water and fluorine on the viscosity of silicic magmas, *Geochim. Cosmochim. Acta*, *68*, 5159–5168.

Gonnermann, H. M., and M. Manga (2003), Explosive volcanism may not be an inevitable consequence of magma fragmentation, *Nature*, *426*, 432–435.

Gonnermann, H. M., and M. Manga (2007), The fluid mechanics inside a volcano, *Annu. Rev. Fluid Mech.*, *39*, 321–356.

Goranson, R. W. (1931), The solubility of water in granite magmas, *Am. J. Sci.*, *22*, 481–502.

Goto, A., H. Taniguchi, and A. Kitakaze (2005), Viscosity measurements of hydrous rhyolitic melts using the fiber elongation method, *Bull. Volcanol.*, *67*, 590–596.

Gottsmann, J., D. Giordano, and D. B. Dingwell (2002), Predicting shear viscosity during volcanic processes at the glass transition: A calorimetric calibration, *Earth Planet. Sci. Lett.*, *198*, 417–427.

Hamilton, D. L., C. W. Burnham, and E. F. Osborn (1964), The solubility of water and effects of oxygen fugacity and water content on crystallization in mafic magmas, *J. Petrol.*, *5*, 21–39.

Hess, K., and D. B. Dingwell (1996), Viscosities of hydrous leucogranitic melts: A non-Arrhenian model, *Am. Mineral.*, *81*, 1297–1300.

Hess, K. U., D. B. Dingwell, and S. L. Webb (1995), The influence of excess alkalis on the viscosity of a haplogranitic melt, *Am. Mineral.*, *80*, 297–304.

Hess, K. U., D. B. Dingwell, C. Gennaro, and V. Mincione (2001), Viscosity-temperature behaviour of dry melts in the Qz-Ab-Or system, *Chem. Geol.*, *174*, 133–142.

Holloway, J. R., and J. G. Blank (1994), Application of experimental results to C-O-H series in natural melts, *Rev. Mineral.*, *30*, 187–230.

Holtz, F., H. Behrens, D. B. Dingwell, and R. P. Taylor (1992), Water solubility in aluminosilicate melts of haplogranite composition at 2 kbar, *Chem. Geol.*, *96*, 289–302.

Holtz, F., H. Behrens, D. B. Dingwell, and W. Johannes (1995), H_2O solubility in haplogranitic melts: Compositional, pressure, and temperature dependence, *Am. Mineral.*, *80*, 94–108.

Holtz, F., J. Roux, S. Ohlhorst, H. Behrens, and F. Schulze (1999), The effect of silica and water on the viscosity of hydrous quartzofelspathic melts, *Am. Mineral.*, *84*, 27–36.

Houser, C. A., J. S. Herman, I. S. T. Tsong, W. B. White, and W. A. Lanford (1980), Sodium-hydrogen interdiffusion in sodium silicate glasses, *J. Non Cryst. Solids*, *41*, 89–98.

Hui, H., and Y. Zhang (2007), Toward a general viscosity equation for natural anhydrous and hydrous silicate melts, *Geochim. Cosmochim. Acta*, *71*, 403–416.

Ichihara, M., D. Rittel, and B. Sturtevant (2002), Fragmentation of a porous viscoelastic material: Implications to magma fragmen-

tation, *J. Geophys. Res.*, *107*(B10), 2229, doi:10.1029/2001JB000591.
Ihinger, P. D. (1991), An experimental study of the interaction of water with granitic melt, report, 190 pp., Calif. Inst. of Technol., Pasadena.
Ihinger, P. D., R. L. Hervig, and P. F. McMillan (1994), Analytical methods for volatiles in glasses, *Rev. Mineral.*, *30*, 67–121.
Jambon, A. (1979), Diffusion of water in a granitic melt: An experimental study, in *Year Book Carnegie Inst Washington*, *78*, 352–355.
Jambon, A., Y. Zhang, and E. M. Stolper (1992), Experimental dehydration of natural obsidian and estimation of D_{H_2O} at low water contents, *Geochim. Cosmochim. Acta*, *56*, 2931–2935.
Kadik, A. A., O. A. Lukanin, Y. B. Lebedev, and E. Y. Korovushkina (1972), Solubility of H_2O and CO_2 in granite and basalt melts at high pressures, *Geochem. Inst.*, *9*, 1041–1050.
Karsten, J. L., J. R. Holloway, and J. R. Delaney (1982), Ion microprobe studies of water in silicate melts: Temperature-dependent water diffusion in obsidian, *Earth Planet. Sci. Lett.*, *59*, 420–428.
Khitarov, N. I., and A. A. Kadik (1973), Water and carbon dioxide in magmatic melts and peculiarities of the melting process, *Contrib. Mineral. Petrol.*, *41*, 205–215.
Koyaguchi, T., and N. K. Mitani (2005), A theoretical model for fragmentation of viscous bubbly magmas in shock tubes, *J. Geophys. Res.*, *110*, B10202, doi:10.1029/2004JB003513.
Kushiro, I., H. S. Yoder, and B. O. Mysen (1976), Viscosities of basalt and andesite melts at high pressures, *J. Geophys. Res.*, *81*, 6351–6356.
Lanford, W. A., K. Davis, P. Lamarche, T. Laursen, R. Groleau, and R. H. Doremus (1979), Hydration of soda-lime glass, *J. Non Cryst. Solids*, *33*, 249–265.
Lange, R. A. (1994), The effect of H_2O, CO_2 and F on the density and viscosity of silicate melts, *Rev. Mineral.*, *30*, 331–369.
Leschik, M., G. Heide, G. H. Frischat, H. Behrens, M. Wiedenbeck, N. Wagner, K. Heide, H. Geissler, and U. Reinholz (2004), Determination of H_2O and D_2O contents in rhyolitic glasses, *Phys. Chem. Glasses*, *45*, 238–251.
Liebske, C., H. Behrens, F. Holtz, and R. A. Lange (2003), The influence of pressure and composition on the viscosity of andesitic melts, *Geochim. Cosmochim. Acta*, *67*, 473–485.
Liu, Y., Y. Zhang, and H. Behrens (2004), H_2O diffusion in dacitic melt, *Chem. Geol.*, *209*, 327–340.
Liu, Y., Y. Zhang, and H. Behrens (2005), Solubility of H_2O in rhyolitic melts at low pressures and a new empirical model for mixed H_2O-CO_2 solubility in rhyolitic melts, *J. Volcanol. Geotherm. Res.*, *143*, 219–235.
Llewellin, E. W., and M. Manga (2005), Bubble suspension rheology and implications for conduit flow, *J. Volcanol. Geotherm. Res.*, *143*, 205–217.
Lux, G. (1987), The behavior of noble gases in silicate liquids: Solution, diffusion, bubbles and surface effects, with applications to natural samples, *Geochim. Cosmochim. Acta*, *51*, 1549–1560.
Mader, H. M., Y. Zhang, J. C. Phillips, R. S. J. Sparks, B. Sturtevant, and E. M. Stolper (1994), Experimental simulations of explosive degassing of magma, *Nature*, *372*, 85–88.
Mader, H. M., J. C. Phillips, R. S. J. Sparks, and B. Sturtevant (1996), Dynamics of explosive degassing of magma: Observations of fragmenting two-phase flows, *J. Geophys. Res.*, *101*, 5547–5560.
Mader, H. M., E. E. Brodsky, D. Howard, and B. Sturtevant (1997), Laboratory simulations of sustained volcanic eruptions, *Nature*, *388*, 462–464.
Majewski, E., and D. Walker (1998), S diffusivity in Fe-Ni-S-P melts, *Earth Planet. Sci. Lett.*, *160*, 823–830.
Mandeville, C. W., J. D. Webster, M. J. Rutherford, B. E. Taylor, A. Timbal, and K. Faure (2002), Determination of molar absorptivities of infrared absorption bands of H_2O in andesitic glasses, *Am. Mineral.*, *87*, 813–821.
Mangan, M., and T. Sisson (2000), Delayed, disequilibrium degassing in rhyolitic magma: Decompression experiments and implications for explosive volcanism, *Earth Planet. Sci. Lett.*, *183*, 441–455.
Matsuda, J.-I., K. Matsubara, H. Yajima, and K. Yamamoto (1989), Anomalous Ne enrichment in obsidians and Darwin glass: Diffusion of noble gases in silica-rich glasses, *Geochim. Cosmochim. Acta*, *53*, 3025–3033.
McBirney, A. R., and T. Murase (1970), Factors governing the formation of pyroclastic rocks, *Bull. Volcanol.*, *34*, 372–384.
Moore, G., T. Vennemann, and I. S. E. Carmichael (1995), The solubility of water in natural silicate melts to 2 kilobars, *Geology*, *23*, 1009–1102.
Moore, G., T. Vennemann, and I. S. E. Carmichael (1998), An empirical model for the solubility of H_2O in magmas to 3 kilobars, *Am. Mineral.*, *83*, 36–42.
Mueller, S., O. Melnik, O. Spieler, B. Sheu, and D. B. Dingwell (2005), Permeability and degassing of dome lavas undergoing rapid decompression: An experimental determination, *Bull. Volcanol.*, *67*, 526–538.
Namiki, A., and M. Manga (2005), Response of a bubble bearing viscoelastic fluid to rapid decompression: Implications for explosive volcanic eruptions, *Earth Planet. Sci. Lett.*, *236*, 269–284.
Neuville, D. R., P. Courtial, D. B. Dingwell, and P. Richet (1993), Thermodynamic and rheological properties of rhyolite and andesite melts, *Contrib. Mineral. Petrol.*, *113*, 572–581.
Newman, S., and J. B. Lowenstern (2002), VOLATILECALC: A silicate melt-H_2O-CO_2 solution model written in Visual Basic for Excel, *Comput. Geosci.*, *28*, 597–604.
Newman, S., E. M. Stolper, and S. Epstein (1986), Measurement of water in rhyolitic glasses: Calibration of an infrared spectroscopic technique, *Am. Mineral.*, *71*, 1527–1541.
Nogami, M., and M. Tomozawa (1984), Diffusion of water in high silica glasses at low temperature, *Phys. Chem. Glasses*, *25*, 82–85.
Nowak, M., and H. Behrens (1995), The speciation of water in haplogranitic glasses and melts determined by in situ near infrared spectroscopy, *Geochim. Cosmochim.*, *59*, 3445–3450.
Nowak, M., and H. Behrens (1997), An experimental investigation on diffusion of water in haplogranitic melts, *Contrib. Mineral. Petrol.*, *126*, 365–376.
Nowak, M., D. Schreen, and K. Spickenbom (2004), Argon and CO_2 on the race track in silicate melts: A tool for the development of a CO_2 speciation and diffusion model, *Geochim. Cosmochim. Acta*, *68*, 5127–5138.
Oehler, A., and M. Tomozawa (2004), Water diffusion into silica glass at a low temperature under high water vapor pressure, *J. Non Cryst. Solids*, *347*, 211–219.
Ohlhorst, S., H. Behrens, and F. Holtz (2001), Compositional dependence of molar absorptivities of near-infrared OH- and H_2O bands in rhyolitic to basaltic glasses, *Chem. Geol.*, *174*, 5–20.
Okumura, S., and S. Nakashima (2004), Water diffusivity in rhyolitic glasses as determined by in situ IR spectroscopy, *Phys. Chem. Minerals*, *31*, 183–189.
Okumura, S., and S. Nakashima (2006), Water diffusion in basaltic to dacitic glasses, *Chem. Geol.*, *227*, 70–82.
Papale, P. (1997), Modeling of the solubility of a one-component H_2O or CO_2 fluid in silicate liquids, *Contrib. Mineral. Petrol.*, *126*, 237–251.
Papale, P. (1999a), Modeling of the solubility of a two-component H_2O + CO_2 fluid in silicate liquids, *Am. Mineral.*, *84*, 477–492.
Papale, P. (1999b), Strain-induced magma fragmentation in explosive eruptions, *Nature*, *397*, 425–428.
Papale, P., R. Moretti, and D. Barbato (2006), The compositional dependence of the saturation surface of H_2O + CO_2 fluids in silicate melts, *Chem. Geol.*, *229*, 78–95.
Perkins, E. H., and D. R. Begeal (1971), Diffusion and permeation of He, Ne, Ar, Kr, and D_2 through silicon oxide thin films, *J. Chem. Phys.*, *54*, 1683–1694.

Persikov, E. S. (1991), The viscosity of magmatic liquids: Experiment, generalized patterns. A model for calculation and prediction. Applications, in *Physical Chemistry of Magmas*, vol. 9, edited by L. L. Perchuk and I. Kushiro, pp. 1–40, Springer, New York.

Persikov, E. S., M. B. Epelbaum, and P. G. Bukhtiyarov (1986), The viscosity of a granite magma interacting with an aqueous chloride fluid, *Geochem. Int.*, *23*, 21–30.

Petford, N. (2003), Rheology of granitic magmas during ascent and emplacement, *Annu. Rev. Earth Planet. Sci.*, *31*, 399–427.

Proussevitch, A. A., and D. L. Sahagian (1998), Dynamics and energetics of bubble growth in magmas: Analytical formulation and numerical modeling, *J. Geophys. Res.*, *103*, 18,223–18,251.

Reynolds, M. B. (1957), Diffusion of argon in a potassium-lime-silica glass, *J. Am. Ceram. Soc.*, *40*, 395–398.

Richet, P., A. Lejeune, F. Holtz, and J. Roux (1996), Water and the viscosity of andesitic melts, *Chem. Geol.*, *128*, 185–197.

Romano, C., J. E. Mungall, T. Sharp, and D. B. Dingwell (1996), Tensile strengths of hydrous vesicular glasses: An experimental study, *Am. Mineral.*, *81*, 1148–1154.

Romano, C., D. Giordano, P. Papale, V. Mincione, D. B. Dingwell, and M. Rossi (2003), The dry and hydrous viscosities of alkaline melts from Vesuvius and Phlegrean fields, *Chem. Geol.*, *202*, 23–38.

Roselieb, K., W. Rammensee, H. Buttner, and M. Rosenhauer (1992), Solubility and diffusion of noble gases in vitreous albite, *Chem. Geol.*, *96*, 241–266.

Roselieb, K., W. Rammensee, H. Buttner, and M. Rosenhauer (1995), Diffusion of noble gases in melts of the system SiO_2-$NaAlSi_2O_6$, *Chem. Geol.*, *120*, 1–13.

Roselieb, K., H. Buttner, U. Eicke, U. Kohler, and M. Rosenhauer (1996), Pressure dependence of Ar and Kr diffusion in a jadeite melt, *Chem. Geol.*, *128*, 207–216.

Russell, J. K., and D. Giordano (2005), A model for silicate melt viscosity in the system $CaMgSi_2O_6$-$CaAl_2Si_2O_8$-$NaAlSi_3O_8$, *Geochim. Cosmochim. Acta*, *69*, 5333–5349.

Sato, H., T. Fujii, and S. Nakada (1992), Crumbling of dacite dome lava and generation of pyroclastic flows at Unzen volcano, *Nature*, *360*, 664–666.

Scaillet, B., F. Holtz, M. Pichavant, and M. Schmidt (1996), Viscosity of Himalayan leucogranites: Implications for mechanisms of granitic magma ascent, *J. Geophys. Res.*, *101*, 27,691–27,699.

Schmidt, B. C., F. Holtz, and M. Pichavant (1999), Water solubility in haplogranitic melts coexisting with H_2O-H_2 fluids, *Contrib. Mineral. Petrol.*, *136*, 213–224.

Schulze, F., H. Behrens, F. Holtz, J. Roux, and W. Johannes (1996), The influence of H_2O on the viscosity of a haplogranitic melt, *Am. Mineral.*, *81*, 1155–1165.

Shaw, H. R. (1963), Obsidian-H_2O viscosities at 1000 and 2000 bars in the temperature range 700° to 900°C, *J. Geophys. Res.*, *68*, 6337–6343.

Shaw, H. R. (1972), Viscosities of magmatic silicate liquids: An empirical method of prediction, *Am. J. Sci.*, *272*, 870–893.

Shaw, H. R. (1974), Diffusion of H_2O in granitic liquids: part I. Experimental data; part II. Mass transfer in magma chambers, in *Geochemical Transport and Kinetics*, edited by A. W. Hofmann et al., *Carnegie Inst. Washington Publ.*, *634*, 139–170.

Shen, A., and H. Keppler (1995), Infrared spectroscopy of hydrous silicate melts to 1000°C and 10 kbar: Direct observation of H_2O speciation in a diamond-anvil cell, *Am. Mineral.*, *80*, 1335–1338.

Sierralta, M., M. Nowak, and H. Keppler (2002), The influence of bulk composition on the diffusivity of carbon dioxide in Na aluminosilicate melts, *Am. Mineral.*, *87*, 1710–1716.

Silver, L., and E. Stolper (1985), A thermodynamic model for hydrous silicate melts, *J. Geol.*, *93*, 161–178.

Silver, L., P. D. Ihinger, and E. Stolper (1990), The influence of bulk composition on the speciation of water in silicate glasses, *Contrib. Mineral. Petrol.*, *104*, 142–162.

Simmons, J. H. (1998), What is so exciting about non-linear viscous flow in glass, molecular dynamics simulations of brittle fracture and semiconductor-glass quantum composites, *J. Non Cryst. Solids*, *239*, 1–15.

Spera, F. J. (2000), Physical properties of magmas, in *Encyclopedia of Volcanoes*, edited by H. Sigurdsson, pp. 171–190, Academic, San Diego, Calif.

Spieler, O., B. Kennedy, U. Kueppers, D. B. Dingwell, B. Scheu, and J. Taddeucci (2004), The fragmentation threshold of pyroclastic rocks, *Earth Planet. Sci. Lett.*, *226*, 139–148.

Stanton, T. R., J. R. Holloway, R. L. Hervig, and E. Stolper (1985), Isotope effect on water diffusivity in silicic melts: An ion microprobe and infrared analysis (abstract), *Eos Trans. AGU*, *66*(46), 1131.

Stein, D. J., and F. J. Spera (1993), Rheometry of a dacitic melt: Experimental results and tests of empirical models for viscosity estimation, *Geophys. Res. Lett.*, *20*, 1923–1926.

Stevenson, R. J., N. S. Bagdassarov, D. B. Dingwell, and C. Romano (1998), The influence of trace amounts of water on the viscosity of rhyolites, *Bull. Volcanol.*, *60*, 89–97.

Stolper, E. M. (1982a), Water in silicate glasses: An infrared spectroscopic study, *Contrib. Mineral. Petrol.*, *81*, 1–17.

Stolper, E. M. (1982b), The speciation of water in silicate melts, *Geochim. Cosmochim. Acta*, *46*, 2609–2620.

Tait, S., R. Thomas, J. Gardner, and C. Jaupert (1998), Constraints on cooling rates and permeabilities of pumices in an explosive eruption jet from colour and magnetic mineralogy, *J. Volcanol. Geotherm. Res.*, *86*, 79–91.

Tamic, N., H. Behrens, and F. Holtz (2001), The solubility of H_2O and CO_2 in rhyolitic melts in equilibrium with a mixed CO_2-H_2O fluid phase, *Chem. Geol.*, *174*, 333–347.

Thomas, N., C. Jaupart, and S. Vergniolle (1994), On the vesicularity of pumice, *J. Geophys. Res.*, *99*, 15,633–15,644.

Tomozawa, M. (1985), Concentration dependence of the diffusion coefficient of water in SiO_2 glass, *Am. Ceram. Soc. Bull.*, *68*, 251–252.

Toplis, M. J., D. B. Dingwell, and T. Lenci (1997), Peraluminous viscosity maxima in Na_2O-Al_2O_3-SiO_2 liquids: The role of triclusters in tectosilicate melts, *Geochim. Cosmochim. Acta*, *61*, 2605–2612.

Tsong, I. S. T., C. A. Houser, and S. S. C. Tong (1980), Depth profiles of interdiffusing species in hydrated glasses, *Phys. Chem. Glasses*, *21*, 197–198.

Wallace, P. J., J. Dufek, A. T. Anderson, and Y. Zhang (2003), Cooling rates of Plinian-fall and pyroclastic-flow deposits in the Bishop Tuff: Inferences from water speciation in quartz-hosted glass inclusions, *Bull. Volcanol.*, *65*, 105–123.

Wang, L., Y. Zhang, and E. J. Essene (1996), Diffusion of the hydrous component in pyrope, *Am. Mineral.*, *81*, 706–718.

Watson, E. B. (1991), Diffusion of dissolved CO_2 and Cl in hydrous silicic to intermediate magmas, *Geochim. Cosmochim. Acta*, *55*, 1897–1902.

Watson, E. B. (1994), Diffusion in volatile-bearing magmas, *Rev. Mineral.*, *30*, 371–411.

Watson, E. B., M. A. Sneeringer, and A. Ross (1982), Diffusion of dissolved carbonate in magmas: Experimental results and applications, *Earth Planet. Sci. Lett.*, *61*, 346–358.

Webb, S. L., and D. B. Dingwell (1990), Non-Newtonian rheology of igneous melts at high stresses and strain rates: Experimental results for rhyolite, andesite, basalt, and nephelinite, *J. Geophys. Res.*, *95*, 15,695–15,701.

Whittington, A., P. Richet, and F. Holtz (2000), Water and the viscosity of depolymerized aluminosilicate melts, *Geochim. Cosmochim. Acta*, *64*, 3725–3736.

Whittington, A., P. Richet, Y. Linard, and F. Holtz (2001), The viscosity of hydrous phonolites and trachytes, *Chem. Geol.*, *174*, 209–223.

Whittington, A., P. Richet, H. Behrens, F. Holtz, and B. Scaillet (2005), Experimental temperature-X(H_2O)-viscosity relationship

for leucogranites and comparison with synthetic silicic liquids, *Geol. Soc. Am. Spec. Pap.*, *389*, 59–71.

Wilson, L. (1980), Relationships between pressure, volatile content and ejecta velocity in three types of volcanic explosions, *J. Volcanol. Geotherm. Res.*, *8*, 297–313.

Winther, K. T., E. B. Watson, and G. M. Korenowski (1998), Magmatic sulfur compounds and sulfur diffusion in albite melt at 1 GPa and 1300–1500°C, *Am. Mineral.*, *83*, 1141–1151.

Withers, A. C., Y. Zhang, and H. Behrens (1999), Reconciliation of experimental results on H_2O speciation in rhyolitic glass using in situ and quenching techniques, *Earth Planet. Sci. Lett.*, *173*, 343–349.

Xu, Z., and Y. Zhang (2002), Quench rates in water, air and liquid nitrogen, and inference of temperature in volcanic eruption columns, *Earth Planet. Sci. Lett.*, *200*, 315–330.

Yamashita, S. (1999), Experimental study of the effect of temperature on water solubility in natural rhyolite melt to 100 MPa, *J. Petrol.*, *40*, 1497–1507.

Zhang, Y. (1994), Reaction kinetics, geospeedometry, and relaxation theory, *Earth Planet. Sci. Lett.*, *122*, 373–391.

Zhang, Y. (1998a), Experimental simulations of gas-driven eruptions: Kinetics of bubble growth and effect of geometry, *Bull. Volcanol.*, *59*, 281–290.

Zhang, Y. (1998b), Mechanical and phase equilibria in inclusion-host systems, *Earth Planet. Sci. Lett.*, *157*, 209–222.

Zhang, Y. (1999a), H_2O in rhyolitic glasses and melts: Measurement, speciation, solubility, and diffusion, *Rev. Geophys.*, *37*, 493–516.

Zhang, Y. (1999b), A criterion for the fragmentation of bubbly magma based on brittle failure theory, *Nature*, *402*, 648–650.

Zhang, Y. (2004), Dynamics of explosive volcanic and lake eruptions (in Chinese), in *Environment, Natural Hazards and Global Tectonics of the Earth*, pp. 39–95, Higher Educ. Press, Beijing.

Zhang, Y., and H. Behrens (2000), H_2O diffusion in rhyolitic melts and glasses, *Chem. Geol.*, *169*, 243–262.

Zhang, Y., and E. M. Stolper (1991), Water diffusion in basaltic melts, *Nature*, *351*, 306–309.

Zhang, Y., and Z. Xu (1995), Atomic radii of noble gas elements in condensed phases, *Am. Mineral.*, *80*, 670–675.

Zhang, Y., and Z. Xu (2007), A long-duration experiment on hydrous species geospeedometer and hydrous melt viscosity, *Geochim. Cosmochim. Acta*, *71*, 5226–5232.

Zhang, Y., E. M. Stolper, and G. J. Wasserburg (1991a), Diffusion of water in rhyolitic glasses, *Geochim. Cosmochim. Acta*, *55*, 441–456.

Zhang, Y., E. M. Stolper, and G. J. Wasserburg (1991b), Diffusion of a multi-species component and its role in the diffusion of water and oxygen in silicates, *Earth Planet. Sci. Lett.*, *103*, 228–240.

Zhang, Y., E. M. Stolper, and P. D. Ihinger (1995), Kinetics of reaction $H_2O + O = 2OH$ in rhyolitic glasses: Preliminary results, *Am. Mineral.*, *80*, 593–612.

Zhang, Y., R. Belcher, P. D. Ihinger, L. Wang, Z. Xu, and S. Newman (1997a), New calibration of infrared measurement of water in rhyolitic glasses, *Geochim. Cosmochim. Acta*, *61*, 3089–3100.

Zhang, Y., J. Jenkins, and Z. Xu (1997b), Kinetics of the reaction $H_2O + O = 2OH$ in rhyolitic glasses upon cooling: Geospeedometry and comparison with glass transition, *Geochim. Cosmochim. Acta*, *61*, 2167–2173.

Zhang, Y., B. Sturtevant, and E. M. Stolper (1997c), Dynamics of gas-driven eruptions: Experimental simulations using CO_2-H_2O-polymer system, *J. Geophys. Res.*, *102*, 3077–3096.

Zhang, Y., Z. Xu, and H. Behrens (2000), Hydrous species geospeedometer in rhyolite: improved calibration and application, *Geochim. Cosmochim. Acta*, *64*, 3347–3355.

Zhang, Y., Z. Xu, and Y. Liu (2003), Viscosity of hydrous rhyolitic melts inferred from kinetic experiments, and a new viscosity model, *Am. Mineral.*, *88*, 1741–1752.

H. Wang and M. Zhu, MOE Laboratory of Orogenic Belts and Crustal Evolution, School of Earth and Space Sciences, Peking University, Beijing 100871, China.

Z. Xu and Y. Zhang, Department of Geological Sciences, University of Michigan, Ann Arbor, MI 48109-1005, USA. (youxue@umich.edu; youxuezhang@pku.edu.cn)